The Impact of Land Surface Properties on Haboobs and Dust Lofting

JENNIE BUKOWSKI[a,b] AND SUSAN C. VAN DEN HEEVER[a]

[a] *Department of Atmospheric Science, Colorado State University, Fort Collins, Colorado*
[b] *Institute of the Environment and Sustainability, University of California, Los Angeles, Los Angeles, California*

(Manuscript received 6 January 2022, in final form 18 May 2022)

ABSTRACT: Haboobs are dust storms formed by strong surface winds in convective storm outflow boundaries, or cold pools, which can loft large quantities of mineral dust as they propagate. Both cold pools and the dust they loft are impacted by land surface properties resulting in complex surface interactions on haboobs. As a result of these additional complexities brought about by surface interactions, it is unclear which surface parameters and physical processes are important for predicting haboob intensity and dust concentrations. Here we applied the Morris one-at-a-time (MOAT) global sensitivity statistical method to an ensemble of 120 idealized simulations of daytime and nighttime haboobs to investigate the land surface properties that affect both dust mobilization and cold pool dynamics. MOAT identifies and ranks the importance of different input factors, which for the prediction of haboob strength and dust concentrations are 1) initial cold pool temperature, 2) surface type (vegetation), 3) soil type (clay content), and 4) soil moisture. The underlying physical mechanisms driving these feedbacks were then analyzed using a traditional one-at-a-time factor analysis. Time of day is significant for determining boundary layer height and dissipation via surface fluxes, leading to shallower, more intense cold pools/haboobs at night. Most of the land parameters modify the cold pool through impacts on surface fluxes, while surface type is dominated by roughness length effects. By ranking the importance of these surface factors, we have identified which variables are most sensitive and must be constrained via observations and data assimilation in numerical dust prediction models.

KEYWORDS: Density currents; Cold pools; Dust or dust storms; Atmosphere-land interaction; Desert meteorology; Aerosols/particulates

1. Introduction

Atmospheric mineral dust is an integral component of the Earth system: it affects Earth's radiation budget (e.g., Slingo et al. 2006; Sokolik and Toon 1996), ice nucleation in clouds (e.g., DeMott et al. 2003; Field et al. 2006; Knopf and Koop 2006; Boose et al. 2016), and biogeochemical cycles and ocean and Amazonian ecosystem fertilization (Martin 1991; Bishop et al. 2002; Mahowald et al. 2005; Jickells and Moore 2015). Dust outbreaks, especially those associated with the cold pools produced by convective storms, are a public safety hazard due to rapid losses in visibility (Baddock et al. 2013; Sprigg 2016; Middleton and Kang 2017) and damages to human respiratory health (Goudie 2014; Middleton 2017).

Haboobs are dust storms that occur as a result of the lofting of dust by the strong lateral winds originating within cold pools. Cold pools are a type of density current and form as precipitation evaporates in dry air below the cloud base of a convective cell or convective system, producing cool, negatively buoyant air that sinks until it hits the ground and spreads out as a distinct cold, rapidly moving air mass (Membery 1985; Roberts and Knippertz 2012; Knippertz and Todd 2012; Cowie et al. 2015; Pantillon et al. 2015, 2016; Drager and van den Heever 2017; Huang et al. 2018). Haboobs quickly loft substantial amounts of dust, can be exceptionally long lived (Flamant et al. 2007; Miller et al. 2008; Roberts and Knippertz 2014; Bukowski and van den Heever 2021), and are a significant source of regional and global dust. Their contributions range from less than 10% of dust emissions in Australia to possibly more than 60% (Bou Karam et al. 2009) in the western Sahel and include a strong seasonal component (Heinold et al. 2013; Bergametti et al. 2017).

Model estimations and forecasts of haboob dust concentrations depend on the accurate representation of cold pools, dust lofting, radiation interactions, and surface factors. Forecasts remain challenging (Knippertz and Todd 2012) due to the scales of cold pool processes (Grant and van den Heever 2016; van den Heever et al. 2021) and the complex, nonlinear interactions between them. Yet, the same surface parameters that affect cold pool dynamics also affect dust mobilization from the surface (Marticorena and Bergametti 1995; Shao et al. 1996, 2002; Shao and Lu 2000; Ginoux et al. 2001). The interaction between the surface, the cold pool, and dust emissions is nonlinear and it is thus ambiguous as to which factors are most important for predicting dust concentrations and other haboob properties. *Here, we will therefore explore the connection between surface properties that affect both dust lofting and cold pool dynamics.*

While wind speed is a major driver of dust emissions, these emissions are modified by the underlying surface (Marticorena and Bergametti 1995; Shao et al. 1996; Shao 2001; Shao and Lu 2000; Ginoux et al. 2001; Darmenova et al. 2009; LeGrand et al. 2019). The physics of dust mobilization from the surface to the atmosphere is complex, and a comprehensive review of how these processes can be quantified is found in Kok et al. (2012).

Supplemental information related to this paper is available at the Journals Online website: https://doi.org/10.1175/JAS-D-22-0001.s1.

Corresponding author: Jennie Bukowski, jenbukow@ucla.edu

DOI: 10.1175/JAS-D-22-0001.1

Dust mobilization mechanisms are necessarily reduced in their complexity for parameterized representation in numerical models, but are still representative of the physical mechanisms that affect emissions. Thus, bulk dust models almost always scale emissions based on the three major land surface factors impacting dust mobilization: soil erodibility and surface type, soil type, and soil moisture content. The direct impact of these different soil scaling factors has been reviewed in detail by Darmenova et al. (2009) and LeGrand et al. (2019).

Yet, these surface parameters are not only important for dust emissions: they are also an integral factor in cold pool dynamics and properties. In this way, land surface properties affect both the mechanics of dust mobilization and the cold pool simultaneously, and this synchronous coupling can feed back on dust emissions and the density current in indirect ways. Thus, this study has two objectives:

1) To identify which land surface parameters, specifically surface type, soil moisture, and soil type, are most significant in predicting haboob dust and propagation.
2) To understand the physical mechanisms that explain why and how these surface properties, important to both dust mobilization and cold pools, affect and feed back on haboob dust lofting and processes.

Most previous literature has focused on either dust or cold pools, but not both, and surprisingly little work has been done on correlating the parameters that affect dust mobilization (soil type, soil moisture, and surface type) with the effects on parent convection or outflow boundaries. Soil type is often studied from the perspective of clay content, whereby soils with higher clay fractions are estimated to loft more dust (Fécan et al. 1999). The clay soil content also affects the partitioning of coarse and fine particles (Marticorena and Bergametti 1995; Shao et al. 1996; Mokhtari et al. 2012) and is important for radiative effects and atmospheric residence time (Kok 2011; Mahowald et al. 2014). Nonetheless, the clay fraction of soil affects its composition, which in turn impacts its thermal conductivity and moisture retention (Abu-Hamdeh 2003) and therefore its interaction with the atmosphere via surface fluxes, which is known to be important for dust uplift (Huang et al. 2018), ingestion into the parent storm (Seigel and van den Heever 2012a), and cold pool dissipation (Bryan and Rotunno 2014; Grant and van den Heever 2016, 2018; Gentine et al. 2016; Drager and van den Heever 2017; Kurowski et al. 2018).

Soil moisture also affects the partitioning of surface fluxes within cold pools (Fast et al. 2019; Drager et al. 2020) and although wet soils loft less dust, the influence and importance of soil moisture in haboobs is unclear. Previous research shows that soil moisture effects reduce cold pool emissions of dust by 15% (Heinold et al. 2013), and on a larger scale, the combined precipitation effect of wet scavenging and soil moisture only affects 9%–25% of total dust uplift potential in the Sahara (Heinold et al. 2013; Bergametti et al. 2016). Furthermore, desert topsoil dries quickly during the day (Belnap et al. 2004) and a large fraction of precipitation evaporates in dry air before reaching the surface (Heinold et al. 2013). In theory, soil moisture may be important for dust mobilization, but the practical significance of soil moisture in desert cold pools and haboobs is still uncertain.

While some studies have investigated soil type and moisture, literature considering the effect of surface type on haboobs is sparse outside of designing erodible soil maps. It is true that erodibility maps can significantly alter modeled dust emissions and radiation (Saleeby et al. 2019) especially on the mesoscale (Walker et al. 2009). Other than scaling by erodibility, surface type is only directly included in some, but not all dust emission equations through a roughness length factor that represents the decrease in dust emissions with taller and/or more roughness elements due to drag and sheltering (Marticorena and Bergametti 1995; MacKinnon et al. 2004; Pierre et al. 2012). Additionally, roughness length has been shown to influence cold pools via changes to sensible and latent heat fluxes (Gentine et al. 2016), which are also affected by the underlying surface vegetation and soil moisture.

In addition to deserts and desertlike environments, drylands, such as short grasslands and cropland/agricultural/grazing rangelands, are also significant local sources of dust (Stout 2001; Lee et al. 2012). In fact, Ginoux et al. (2012) found that 20% of global dust emissions originate from surfaces with vegetation and that anthropogenic dust sources, mainly from agricultural grasslands and croplands, contribute 25% of the global dust budget. Anthropogenic climate change has already led to the desertification of drylands (Burrell et al. 2020) and dust is correlated with drought (Reheis and Urban 2011), which has and is projected to increase as temperatures warm (Bell et al. 2018). Furthermore, there is evidence that desert dust has doubled in the last century (Mahowald et al. 2010) and that emissions have increased in nondesert regions due to climate change and anthropogenic activities, which includes short grasslands (Munson et al. 2011) and agricultural regions (Neff et al. 2008; Brahney et al. 2013). Research on dust emissions in expanded dryland ecosystems is already underrepresented in the literature; understanding how these different surfaces loft and respond to dust in convective outflow boundaries is useful now, but will also be relevant to understanding the transition of surface environments and haboobs in a warming climate.

To complicate matters, the time of day is also significant for determining surface heat fluxes and cold pool propagation (Liu and Moncrieff 2000; Seigel and van den Heever 2012a). Huang et al. (2018) has taken a first step in understanding haboob–surface interactions by investigating how dust uplift changes in response to prescribed and static daytime sensible heat fluxes under the cold pool. They found through idealized simulations that increasing the sensible heat flux warmed the cold pool, but increased the wind speed and dust uplift due to enhanced mixing at the surface. Bukowski and van den Heever (2021) examined the role of interactive surface fluxes and dust radiative effects in a long-lived haboob case study traversing day, evening, and nighttime environments. They found similar surface flux feedbacks, but also noted the importance of nocturnal shifts toward negative sensible heat fluxes and low-level inversions on propagation speed and dust uplift.

With numerous concurrent interactions between dust uplift, the cold pool, and the surface, it is challenging to distinguish which factors are most important for predicting dust concentrations and the properties/dynamics of haboobs. Identifying these factors is critical for interactive dust modeling, including considerations for model setup, the necessary accuracy of model input data, and selecting the most useful observations for data assimilation. *This study seeks to quantify the importance of surface type, soil moisture, and soil type in predicting haboob propagation and dust lofting, and to understand the physics of these haboob–surface feedbacks.* To achieve this, an ensemble of 120 idealized numerical simulations of daytime and nighttime haboobs of varying strengths and surface properties will be analyzed using a global sensitivity technique and one-at-a-time factor separation tests.

2. Idealized case study and model description

a. Model description and physics

Simulations are conducted using the open-source Regional Atmospheric Modeling System version 6.2.11 (Pielke et al. 1992; Cotton et al. 2003; Saleeby and van den Heever 2013). Typically, resolution $O(\sim 100)$ m is necessary to model cold pools both from a numerical convergence standpoint (Bryan et al. 2003; Lebo and Morrison 2015; Jeevanjee 2017) and to represent small-scale heterogeneous cold pool processes (Droegemeier and Wilhelmson 1987; Straka et al. 1993; Bryan et al. 2003; Grant and van den Heever 2016; Hirt et al. 2020; van den Heever et al. 2021); thus, a horizontal grid spacing of 150 m is utilized on a 65 km × 67.5 km domain. The simulations are run in 3D to better represent the turbulent energy cascade in the Kelvin–Helmholtz waves generated in the turbulent wake of the density current (Cantero et al. 2008; Bryan and Rotunno 2014). The vertical grid includes 150 stretched levels with a $\Delta z_{\min} = 50$ m at the surface to a $\Delta z_{\max} = 150$ m aloft, with 50 m being the maximum vertical grid spacing recommended by Grant and van den Heever (2016) for modeling surface cold pool interactions.

Model parameterizations include a Smagorinsky turbulence scheme (Smagorinsky 1963; Lilly 1962; Hill 1974) and the Harrington (1997) radiation scheme, which is updated every minute and can interact with atmospheric aerosol (Stokowski 2005; Saleeby and van den Heever 2013). Model dust scatters and absorbs radiation based on observations from the Saharan Dust Experiment (Haywood et al. 2003) with an index of refraction of $1.53 + 0.0015i$. RAMS is coupled to the interactive Land Ecosystem–Atmosphere Feedback version 3 (LEAF-3) surface model (Walko et al. 2000) where the surface vegetation and soil classes are initialized homogeneously but interact dynamically with the atmosphere via surface fluxes. To simplify the analysis and remove cloud and precipitation effects, no wet microphysics are included. Water vapor is allowed to interact with the land surface and radiation, but it will not condense. Because of the arid environment and associated deep boundary layer, it is unlikely that lift at the cold pool edge will be sufficient to reach the lifted condensation level. Thus, for this idealized cold bubble setup and arid conditions, wet microphysics are unnecessary.

The lateral boundary conditions are cyclic in both the latitudinal and longitudinal direction. Initial conditions for the atmosphere and soil are from ERA5 (C3S 2017) and are horizontally homogeneous with zero background winds and no topography. The reanalysis data are from the Arabian Peninsula on 3 August 2016, at Riyadh which was selected because it represents a well-studied and modeled dust event from the special ACP/AMT issue "Holistic Analysis of Aerosol in Littoral Environments—A Multi-Disciplinary University Research Initiative" (HAALE-MURI) (Miller et al. 2019). Soundings from 0600:00 UTC (0900:00 local) and 1800:00 UTC (2100:00 local) were used to initialize the daytime and nighttime simulations, respectively (Fig. 1). The soundings are representative of the arid interior basin of the Arabian Peninsula, exhibiting dry air aloft and at the surface and a deep planetary boundary layer. The soundings are similar for day and night, although at night the boundary layer is reduced and a stable nocturnal surface layer begins to develop.

The daytime and nighttime simulations are initially integrated for 3 h, each with their respective initial surface conditions, from 0600 to 0900 UTC (0900 to 1200 local) and 1800 to 2100 UTC (2100 to 0000 local), respectively, to allow the planetary boundary layer and surface fluxes to develop/decline. After 3 h, a single cold bubble is released and the model is integrated for another 60 min. A limitation of the single, idealized cold bubble setup is that the cold pools are not continuously forced by a precipitation shaft or its associated downdraft. This setup is therefore an approximation for shorter-lived, isolated precipitating systems and is less valid for longer-lived more organized systems.

The cold bubble is centered horizontally in the domain with a horizontal diameter of 8 km. In the vertical, the bubble is initialized with its lower edge at 150 m AGL and its top at 6 km. In both the vertical and horizontal, the cold bubble perturbation is represented as a cosine squared function with the strongest perturbation in the center decaying away toward ambient conditions at the sphere's edges. The selected cold bubble depth is characteristic of the deep planetary boundary layer and high-based convection typical of this region (Cuesta et al. 2009; Garcia-Carreras et al. 2015). All of the cold pools initially have a positive moisture perturbation of 5.0 g kg^{-1}, based on observations of Saharan density currents (Trzeciak et al. 2017). A summary of the initial cold pool features, simulation setup, and physics options are listed in Table 1.

The simulations are highly, although not perfectly, radially symmetric across the horizontal plane (Fig. 2). Despite small deviations from symmetry occurring due to perturbations in temperature and wind fields from eddy development in the boundary layer, these deviations are small enough to use an azimuthal average from the center of the domain outward to create 2D cross sections (Figs. 3 and 4). After computing the 2D azimuthal average, the time-varying mean environmental state ($\overline{x}_{\text{env}}$) was calculated at each vertical level from a 10-gridpoint average near the edge of the domain. All values are reported as perturbations (x') from this mean

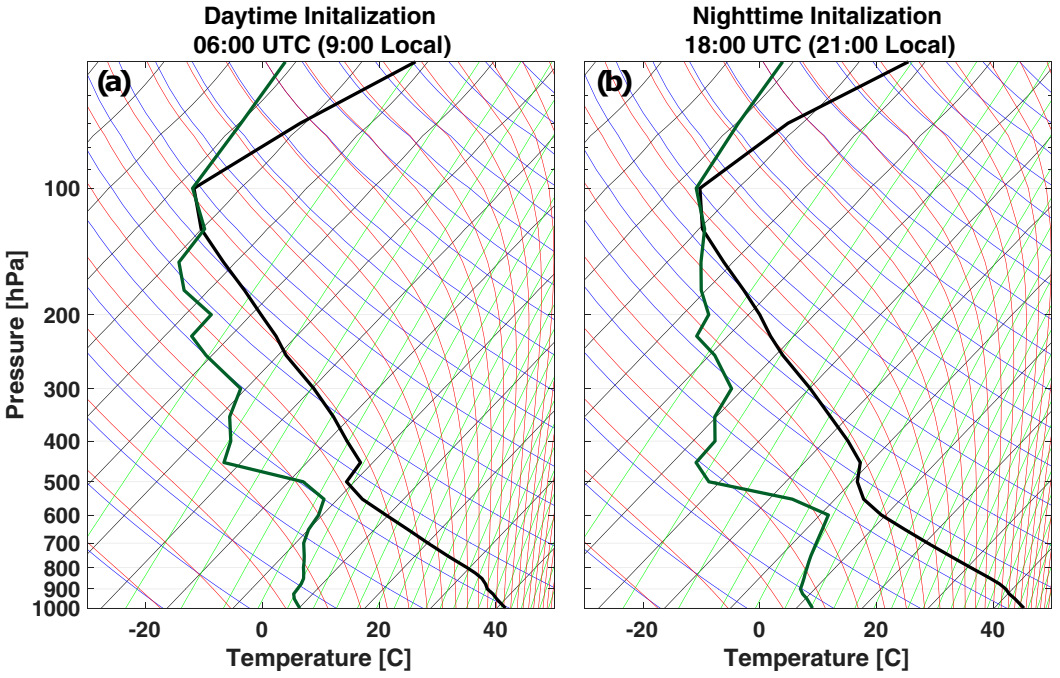

FIG. 1. ERA5 soundings from 3 Aug 2016 at Riyadh, Saudi Arabia, used to initialize the model for the (a) 0600 UTC (0900 local) daytime and (b) 1800 UTC (2100 local) nighttime simulations.

environmental state (i.e., $x' = x - \overline{x}_{\text{env}}$) to account for differences in the development of the boundary layer and surrounding environment based on the surface conditions. Thus, for example, the cold pool perturbation potential temperature (θ'), referenced throughout this paper simply as "cold pool temperature," is calculated as $\theta' = \theta_{\text{cold pool}} - \overline{\theta}_{\text{env}}$.

b. *Dust emission parameterization*

Dust emissions in RAMS (Seigel and van den Heever 2012b; Saleeby and van den Heever 2013) are parameterized [Eq. (1)] based on the GOCART dust scheme (Ginoux et al. 2001, 2004):

$$F_p = CE_{Z_0} s_p U^2 (U - \text{Ut}_{\text{wet}}) \quad \text{if} \quad U > \text{Ut}_{\text{wet}} \ \text{and} \ w_{\text{soil}} < 0.5. \tag{1}$$

In Eq. (1), F_p is the dust flux from the surface (kg m^{-2} s^{-1}) for two dust bins (p) partitioned into a supermicron coarse bin and a submicron fine mode bin by the fractional number s_p (0 to 1), which depends on the clay content of the soil (Alfaro and Gomes 2001; Shao 2001). Other terms are as follows: C is a dimensional factor equal to 1 kg s^2 m^{-5}, U is the 10 m wind speed (m s^{-1}), and Ut_{wet} is the threshold velocity of wind erosion, Ut (m s^{-1}), including a soil moisture correction. Ut_{wet} represents the suppression of dust mobilization in wet soils due to increased cohesive forces, determined empirically to be relative to the clay percentage, %clay, of the soil (Fécan et al. 1999). The dust parameterization is only used if both the near-surface wind speed exceeds the threshold velocity *and* the soil saturation fraction w_{soil} is below 0.5. There is a known disconnect in the GOCART scheme [Eq. (1)] whereby the 10 m wind speed is compared to a threshold value Ut based on friction velocity (LeGrand et al. 2019). Nevertheless, GOCART has tested well against observations in the Weather Research and Forecasting (WRF) Model and this formulation has been retained in its most recent updates (Ukhov et al. 2021). In addition to the other scaling parameters in Eq. (1), E_{Z_0} is the scale factor of the surface roughness Z_0 (cm) (Pierre et al. 2012). Physically, the roughness length affects dust lofting both by shielding erodible soil and reducing the wind momentum transferred to the erodible soil surfaces. E_{Z_0} ranges from 0 to 1 and decreases dust emissions as the total surface roughness due to obstacles (soil, vegetation, pebbles, etc.) increases (Marticorena and Bergametti 1995; Shao and Yang 2005; Marticorena et al. 2006; Xi and Sokolik 2015; Foroutan et al. 2017). In this experiment, the E_{Z_0} scaling factor is employed for all surface types. While some dust schemes employ a second drag partitioning term, $R(Z_0, Z_{0s})$, to model surface roughness effects in the Ut term (e.g., Shao 2001, 2004; Shao et al. 2011; Darmenova et al. 2009; Pierre et al. 2012), Webb et al. (2020) have shown that a single erodibility, or roughness length scaling factor, E_{Z_0}, is sufficient. Hypothetically, if RAMS included both the $R(Z_0, Z_{0s})$ and E_{Z_0} terms, it would enhance the impact surface type has on dust emissions but would not affect the cold pool directly since it only appears in the dust parameterization equations. Including another term that introduces variability into the system would lead to surface type being ranked as more important than what is presented in section 4.

Outside of the dust parameterization, roughness length also affects heat fluxes between the atmosphere and land surface, and hence cold pool intensity. Higher roughness lengths

TABLE 1. Summary of the RAMS model physics and settings.

Model aspect	Setting
Model	Regional Atmospheric Modeling System (RAMS) version 6.11.2 (Pielke et al. 1992; Cotton et al. 2003)
Grid	Single Arakawa C grid (Mesinger and Arakawa 1976)
Δx, Δy, Δz = longitudinal, latitudinal, vertical grid spacing	$\Delta x = \Delta y = 150$ m
nx, ny, nz = number of grid boxes	nx = 430, ny = 450, nz = 150
Δz_{min}, Δz_{max}, $\Delta z_{stretch\_ratio}$ = smallest/largest vertical spacing/stretch ratio	$\Delta z_{min} = 50$ m, $\Delta z_{max} = 150$ m, $\Delta z_{stretch\_ratio} = 1.02$
Model top	19.3 km
	Rayleigh damping over top 14 layers (~2 km)
Time step (Δt)	$\Delta t = 0.5$ s
Integration and output	3 h: Boundary layer development
	1 h: Cold pool
	1-min output frequency
Model start	0600 UTC (0900 local): Daytime
	1800 UTC (2100 local): Nighttime
Microphysics	Water vapor physics only; no condensed water
Turbulence	Smagorinsky (1963) with stability modifications by Lilly (1962) and Hill (1974)
Radiation	Harrington (1997) with added aerosol sensitivity (Stokowski 2005; Saleeby and van den Heever 2013)
Land surface	LEAF-3 (Walko et al. 2000) constant and homogeneous erodible soil fraction
	Constant and homogeneous erodible soil fraction
Lateral boundary conditions	Cyclical
Initialization	Horizontally homogeneous
	Zero background wind
	No topography
Initial and surface conditions	ERA5 from Riyadh, Saudi Arabia
Coriolis	None
Cold pool initialization	Center of domain
z_{cp_start} = lowest height of initial cold pool	Diameter = 8 km
z_{cp_end} = highest height of initial cold pool	$z_{cp\_start} = 150$ m
	$z_{cp\_end} = 6$ km
	+5.0 g kg^{-1} water vapor perturbation

enhance downward momentum transfer at the surface, represented by the surface friction velocity u^* (m s^{-1}), which increases sensible [Eq. (2a)] and latent [Eq. (2b)] heat fluxes (SHF; LHF) in the bulk aerodynamic formulas:

$$\text{SHF} = C_d C_p \rho_{\text{air}} U (T_{\text{sfc}} - T_{\text{air}}), \tag{2a}$$

$$\text{LHF} = C_d C_p \rho_{\text{air}} U (Q_{\text{sfc}} - Q_{\text{air}}). \tag{2b}$$

Here C_d is an aerodynamic bulk transfer coefficient that increases as roughness height increases, C_p is the heat capacity of dry air at constant pressure (J kg^{-1} K^{-1}), ρ_{air} is the density of air (kg m^{-3}), U is the near-surface wind speed (m s^{-1}), and $T_{\text{sfc}}/Q_{\text{sfc}}$ and $T_{\text{air}}/Q_{\text{air}}$ are the temperature and water vapor mixing ratios of the surface and the near-surface air (K, kg kg^{-1}), respectively.

Dust is removed from the atmosphere via dry deposition onto the surface due to gravitational settling (Baron and Willeke 2001; Seinfeld and Pandis 2006; Smith 2007) and dynamical transport via downdrafts. Descriptions of the dust removal mechanisms in RAMS can be found in Saleeby and van den Heever (2013). To first order, stronger winds, drier soils, smoother surfaces, and higher clay fractions will lead to more dust flux to the atmosphere. Because of the U^2 term in Eq. (1), wind speed is the most important parameter in parameterized dust emissions. Nevertheless, as seen in Bukowski and van den Heever (2020), higher-order parameters, such as soil moisture, modulate the effect of wind speed.

3. Ensemble design

a. *Factors of interest*

Based on the literature discussed in section 1, we selected five factors that are likely to influence haboob strength and properties: cold pool temperature, soil moisture, clay soil fraction, surface type, and day versus night. Each of these variables will alter dust emissions and settling, *and* interactions between the cold pool and the land surface. These input parameters are combined into a simulation ensemble using the Morris one-at-a-time (MOAT) technique (Morris 1991; Campolongo et al. 2007), also known as the elementary effects method. A summary of the ensemble design is found in Table 2.

Foremost, the strength of the cold pool relative to its environment determines the cold pool propagation and wind

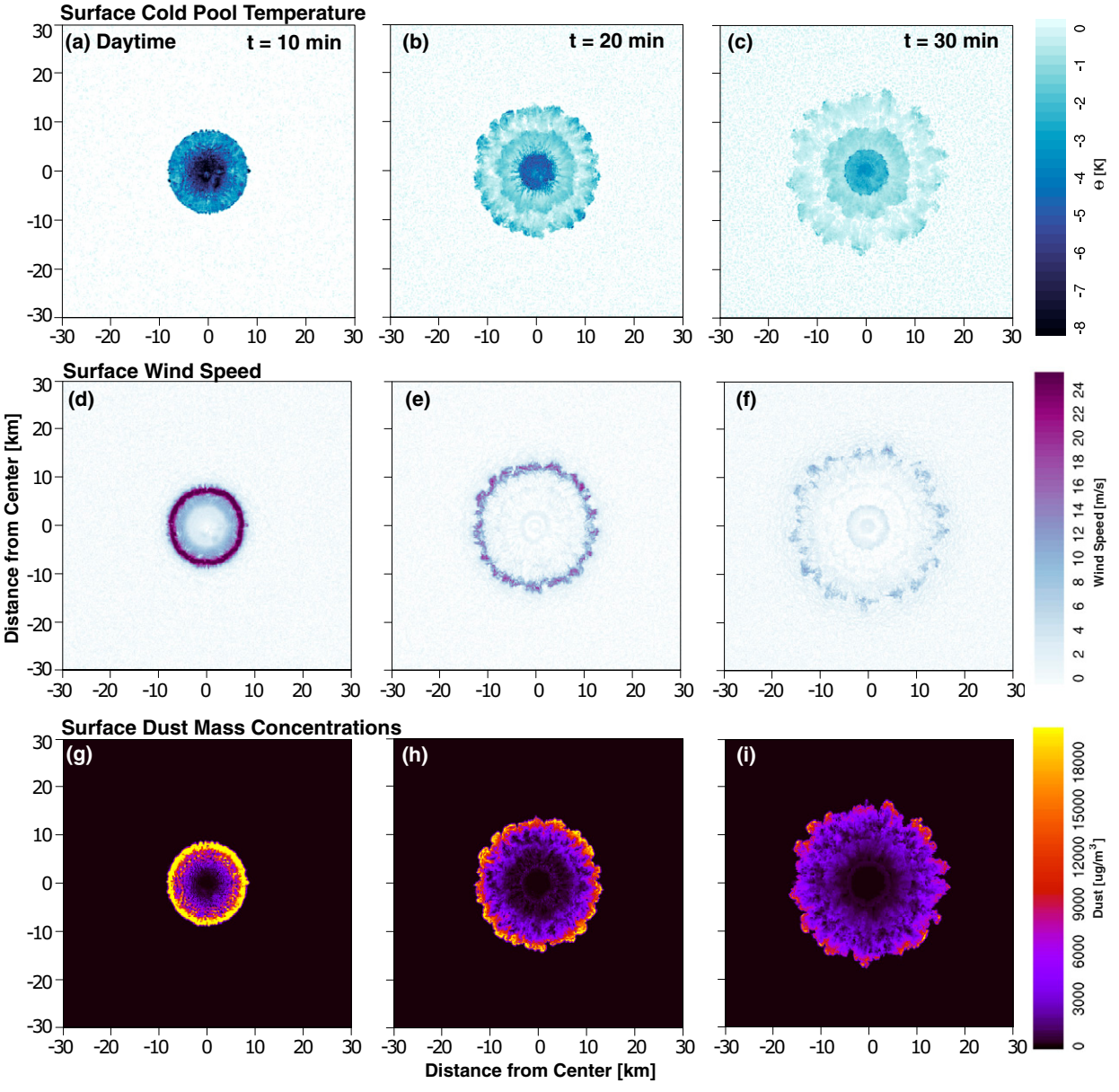

FIG. 2. Plan view example of the first 30 min of the haboob's surface evolution for (a)–(c) cold pool perturbation potential temperature, (d)–(f) horizontal wind speed, and (g)–(i) dust concentrations for the daytime case. The abscissa represents the distance from the center of the domain and therefore the center of the cold pool. This example represents the following initial conditions: 16.6 K cold pool, bare desert surface, clay-type soil (65%), and 27% soil saturation. The nighttime version of this plot can be found in Fig. S1.

speed, which in turn will impact dust flux to the atmosphere [(Eq. (1)]. Cold pool strength and propagation speed are driven by the temperature (and hence density) difference between cold pool air and the environmental air around it and can be estimated with the following equation (Benjamin 1968; Rotunno et al. 1988):

$$V^2 = 2\int_0^H -g\frac{\theta'}{\overline{\theta}_{\text{env}}}\,dz, \tag{3}$$

where V is the theoretical density current propagation speed (m s^{-1}), or intensity, H is the cold pool depth (m) defined by a buoyancy threshold, g is gravitational acceleration (m s^{-2}), dz is the model vertical grid spacing (m), θ' is the cold pool perturbation potential temperature (K) relative to the mean air outside the density current, $\overline{\theta}_{\text{env}}$ (K), with θ' calculated as a simple difference between the environmental air and the cold pool air ($\theta' = \theta_{\text{cold pool}} - \overline{\theta}_{\text{env}}$).

The cold pool temperatures in this experiment range from an initial maximum perturbation aloft of −20 to −10 K. As the cold bubble sinks, it warms; by the time the cold pool reaches the surface, the initial temperature perturbation decreases by ~5 K. This warming reduces the effective surface

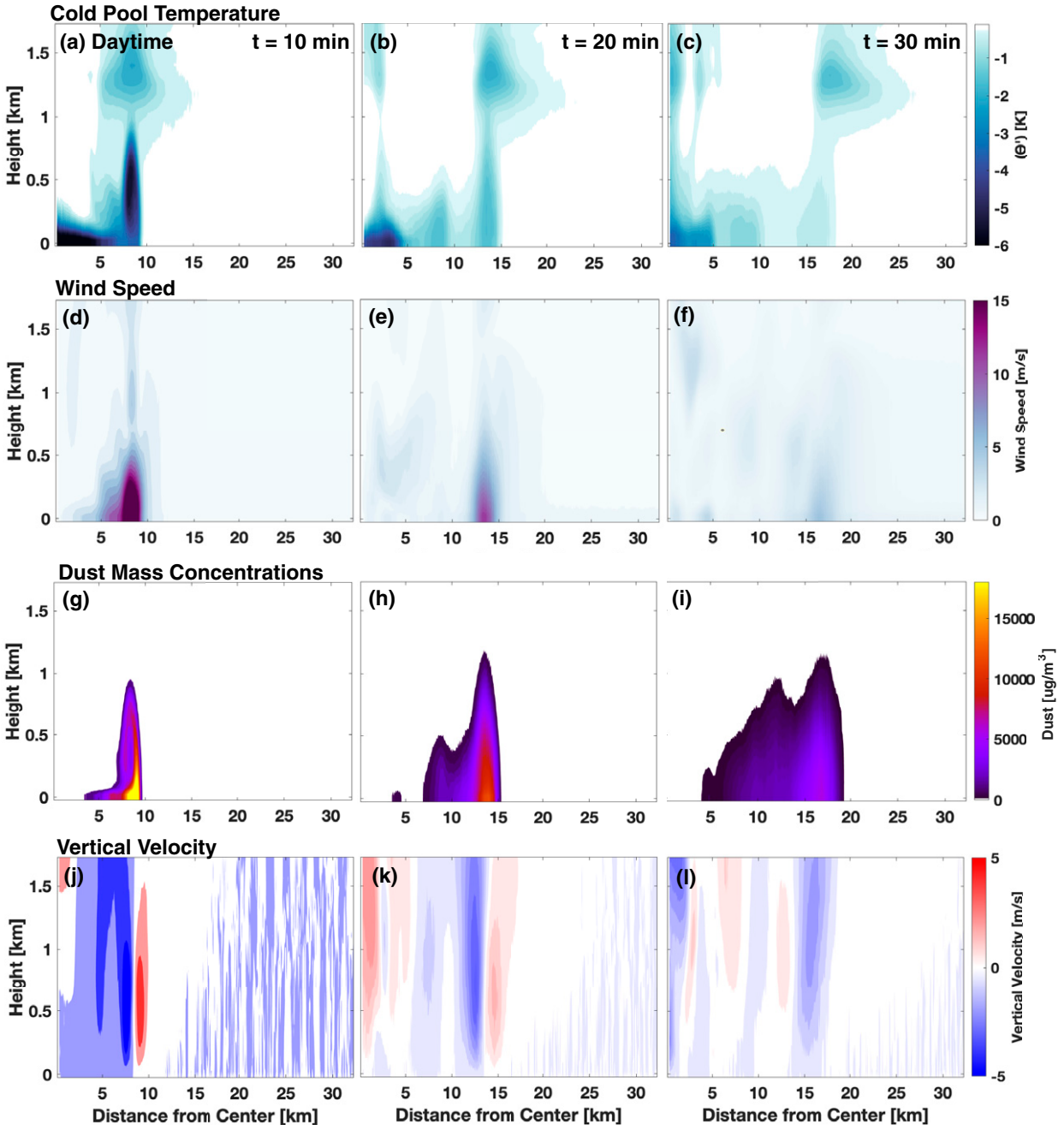

FIG. 3. As in Fig. 2, but a 2D azimuthally averaged cross section instead of a plan view for the daytime case, with the addition of (j)–(l) vertical velocity.

cold pool temperatures to a range of −15 to −5 K and was designed to match observations and modeling studies of surface cold pool temperatures in the Sahara (Lawson 1971; Knippertz et al. 2007, 2009; Emmel et al. 2010; Bou Karam et al. 2014; Provod et al. 2016).

Two separate soil properties were tested, including soil moisture and soil clay fraction. Soil moisture was simulated as a percent of soil saturation and was set to the same value at all soil depths. Values were initialized between 20% and 40% and were selected because they represent conditions where cold pools are entering environments where it has and has not previously rained and moistened the soil, respectively, or where wet soils have begun to dry out under arid conditions (Bergametti et al. 2016). The soil moisture range is also deliberately set to match those in RAMS, which limits dust emissions to soil moistures of 15%–50%. The prescribed soil

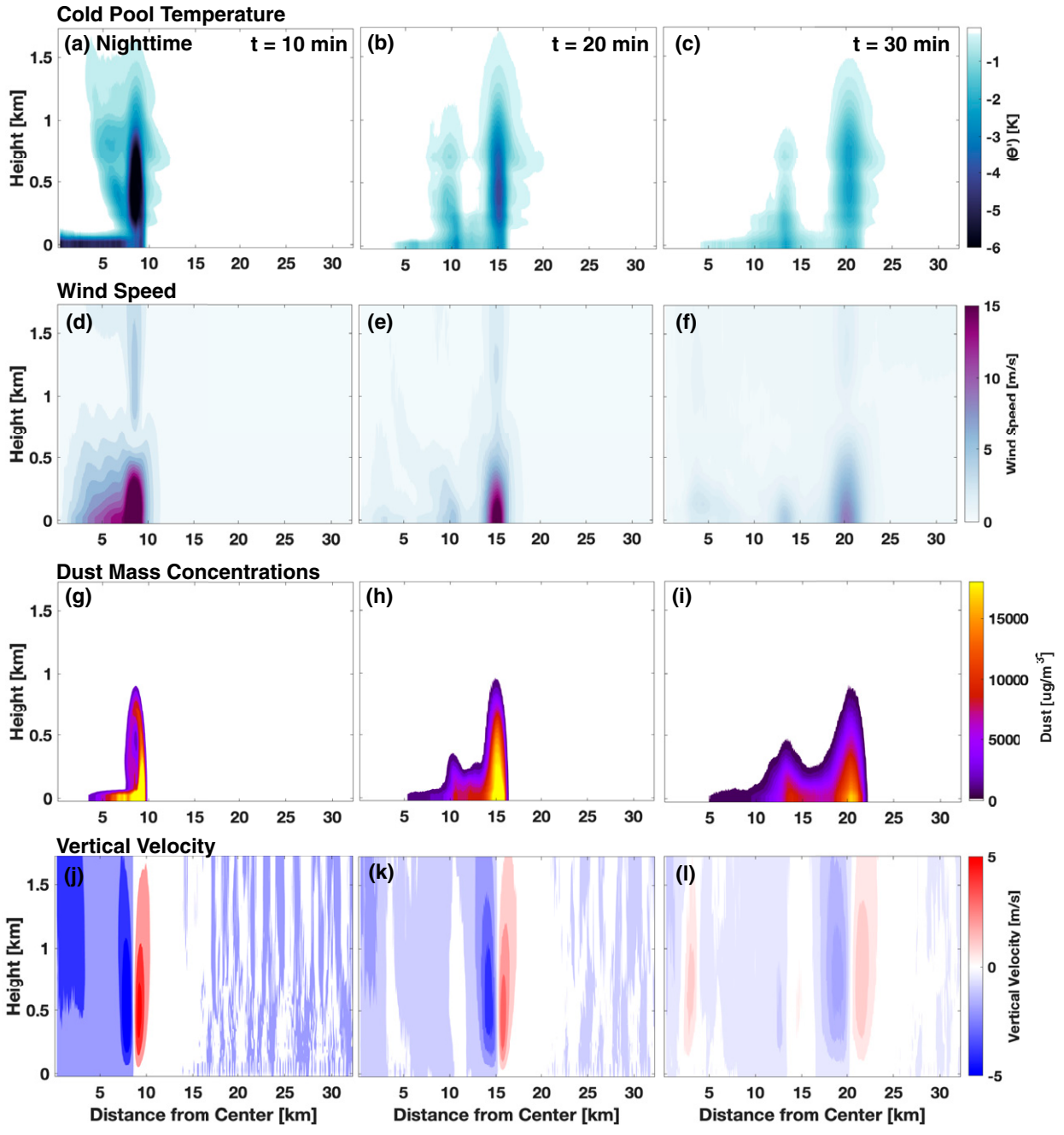

FIG. 4. As in Fig. 3, but for the nighttime case.

moistures in the ensemble are not high enough to completely inhibit dust lofting (>50%), which means the effects studied here only represent the role of soil moisture as a modulating land surface factor in dry dust-producing conditions. The clay fraction of soil was set to 65% for clay type soil, 57% for silty clay loam, 48% for clay loam, and 40% for silty loam and were based on erodibility measurements from arid soils in the Middle East (Vaezi et al. 2016; Gyamfi et al. 2016), which show clay and silt type soils as most likely to erode and loft dust.

Four different dust-emitting surface types were selected, including desert, semidesert, short grasslands, and agricultural crop–grassland. The Arabian Peninsula is best represented by a desert or semidesert scrub surface (Sayre et al. 2020), although other major dust sources including the Sahara, Gobi, and western Australian deserts (Tanaka and Chiba 2006) are bounded by transitional grasslands and croplands (Sayre et al. 2020), in addition to vegetated and agricultural lands being large sources of local dust (Ginoux et al. 2012; Stout 2001;

TABLE 2. Summary of the range in values tested for the input parameters included in the ensemble.

RAMS/MOAT simulation ensemble				
Cold pool temperature (K)	−10	−13.33	−16.67	−20
Soil moisture (% saturated)	20%	26.67%	33.33%	40%
Soil type/clay fraction	Clay/65%	Silty clay loam/57%	Clay loam/48%	Silty loam/40%
Surface type	Desert	Semidesert	Short grassland	Crop–grassland
Day vs night	1200 local time	0000 local time		

Lee et al. 2012). Each surface type has a unique representation in the LEAF-3 interactive land surface model, including albedo, evapotranspiration, surface–air heat exchanges, and surface roughness (0.001, 0.066, 0.034, 0.100 m), which depends on the combination of soil roughness (0.001 m), vegetation height (0.0, 0.7, 0.3, 1.0 m), and fractional vegetation coverage (0.0, 0.2, 0.75, 0.85). In reality, each surface type is representative of a distinct environment that may differ from the reference sounding used here. However, the same sounding was used for each surface type to remove an additional factor of influence and because it is unclear how or if a change in environment could be combined with the MOAT technique.

Last, the difference resulting from the time of day was examined by running two separate suites of simulations to represent a daytime and a nighttime case. In the day, SHF will be positive (surface to air), whereas at night the sign can change to negative heat fluxes (air to surface), which may alter both the cold pool propagation and longevity (Bukowski and van den Heever 2021). Additionally, environmental stability differs between day and night, with the nighttime case being more statically stable, which can affect cold pool propagation speeds (Liu and Moncrieff 2000; Seigel and van den Heever 2012a).

b. *MOAT sensitivity analysis*

The MOAT method (Morris 1991; Campolongo et al. 2007) is used to rank which of the surface input factors (cold pool temperature, soil moisture, clay soil fraction, and surface type) are most important for predicting model output variables (e.g., wind speed, dust concentration, SHF). In addition to representing input–output relationships, MOAT is utilized to select appropriate combinations of surface factors and cold pool temperatures for the simulations, reduce the computational burden, and estimate the nonlinearity across input and output variables. Each of these features of MOAT and modifications made to the statistical algorithm are discussed below.

1) IDENTIFYING AND RANKING INPUT–OUTPUT RELATIONSHIPS

MOAT is a global sensitivity analysis technique, which relates uncertain input parameters in a system to output values by perturbing a single input factor at a time. The statistical algorithm then quantifies the overall influence of the input factor on designated model output variables (μ^*) and ranks the input parameters in terms of their importance via the magnitude of μ^*, with higher values of μ^* designating stronger influence. It is important to reiterate that the purpose of MOAT and other global sensitivity methods is to determine how an initial input factor's value affects the output of a variable. Here the input factors we will test are initial cold pool temperature, soil moisture, soil type, and surface type, while the output variables will relate to haboob intensity (i.e., cold pool perturbation temperature) and dust concentrations. While the sensitivity can be calculated at different times in the simulation, these methods only reflect the effect of the initial values on the solution. Temporal correlations outside of initial values and attribution of physical mechanisms for the observed results in MOAT must be assessed by comparing the output of the one-at-a-time simulations to each other (section 4c).

2) INITIAL CONDITIONS AND REDUCING THE NUMBER OF SIMULATIONS

In addition to estimating interactions across input factors, MOAT reduces the total number of model runs compared to traditional factor analysis methods, making it one of the most efficient global sensitivity techniques (Sarrazin et al. 2016). MOAT is a multiple start perturbation method (Pianosi et al. 2016), where each "start," or initial condition, is randomly selected from a uniform grid of input parameter values and then follows a trajectory through the parameter value space by moving a discrete amount one factor at a time. This process is repeated R number of times to eliminate bias resulting from the initial condition influencing the trajectory. A local sensitivity is calculated for each trajectory and are then all combined to create a global sensitivity estimate of the full input parameter space, without having to test all possible combinations. Twelve trajectories were run for this study, which falls within the range required to reach solution convergence (Saltelli et al. 2004) and was informed by the number of trajectories (R) used in other Earth system modeling studies (e.g., Covey et al. 2013). Trajectory convergence was identified by plotting μ^* as a function of the number of trajectories (Fig. S4 in the online supplemental material) and locating the number R where μ^* approaches an invariant singular value. In traditional one-at-a-time methods, the number of simulations scales as N^k, where N is the number of input parameters and k is the number of values tested for each input parameter. Moreover, including a separate daytime and nighttime ensemble for this study doubles the number of model runs ($2N^k$). Here, $N = 4$ input factors perturbed with $k = 4$ values requires 512 simulations. The MOAT trajectory approach is independent of k and requires only $R(N + 1)$ model runs, or $2R(N + 1)$ for our study. Thus, with $R = 12$ trajectories, MOAT reduces the ensemble to 120 simulations.

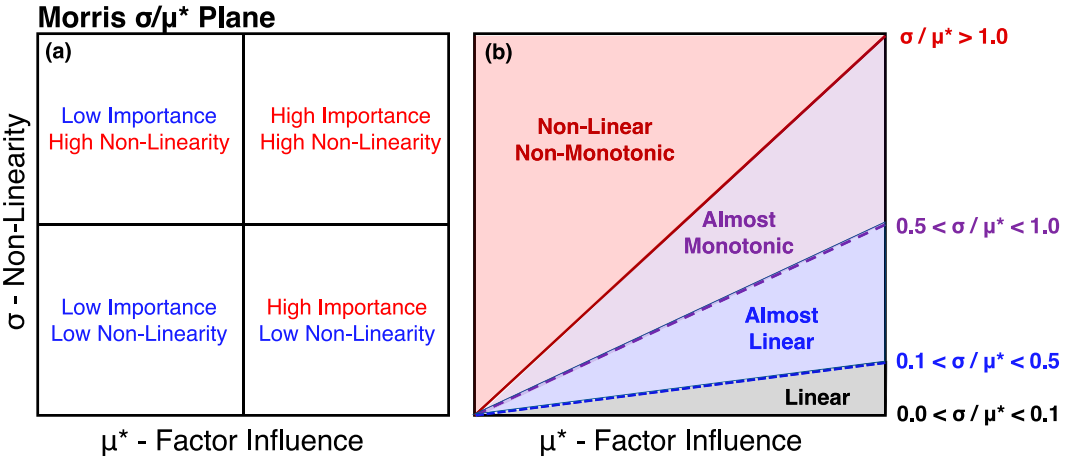

FIG. 5. Interpretation and visualization of the MOAT sensitivity analysis using the σ_s–μ_s^* plane for (a) the input factor importance (μ_s^*) and (b) the factor's nonlinearity (σ_s). The plot in (b) indicates how the slope (σ_s/μ_s^*) can represent the relationship between an input factor and output variable, including being linear (black), almost linear (blue), almost monotonic (purple), and nonlinear and/or nonmonotonic (red) relationships, respectively.

3) ESTIMATING THE NONLINEARITY OF INPUT–OUTPUT RELATIONSHIPS

MOAT is unique in that it can estimate nonlinearity and interactions between input factors in the system (σ), with higher values of σ indicating a stronger dependence on the values of other input factors, or more interactions between factors. The σ–μ^* plane is used to visualize the results (Fig. 5), with each quadrant representing the four possible combinations of high/low importance (μ^*) and high/low nonlinearity (σ) (Fig. 5a). The ratio of σ/μ^* also provides information on the correlation between the input parameter and the output variable (Garcia Sanchez et al. 2014) and whether the relationship is linear ($\sigma/\mu^* < 0.1$), monotonic ($0.1 < \sigma/\mu^* < 0.5$), almost monotonic ($0.5 < \sigma/\mu^* < 1.0$), or nonlinear or nonmonotonic ($\sigma/\mu^* > 1.0$) (Fig. 5b).

4) MODIFICATIONS TO THE MOAT ALGORITHM

All MOAT calculations were performed with the Sensitivity Analysis for Everybody (SAFE) toolbox (Pianosi et al. 2015), which uses the Campolongo et al. (2007) absolute value modification to Morris (1991). Because the units of μ^* are unique to each variable, we have made our own modification to μ^* to report these values in a standardized form (μ_s^*). Here, μ^* is scaled from 0 to 1 to turn MOAT into a factor ranking tool by allowing a direct comparison across factors regardless of their units. This is accomplished by dividing μ^* and σ by the maximum μ^* in each 10-min time frame to yield μ_s^* and σ_s. Here, $\mu_s^* = 1$ indicates an input parameter is critically important, while $\mu_s^* = 0$ indicates zero prognostic significance on the output variable. Values of μ_s^* between 0 and 1 represent importance relative to 1 (e.g., $\mu_s^* = 0.9$ means the input factor is 90% as important as the most important input parameter). Unlike some other variance-based methods, the individual μ_s^* numbers do not sum to 1 and multiple input factors can have the same value if they are equally as important. While μ_s^* ranges from 0 to 1, the only limitation on σ_s is that it must be positive; highly nonlinear situations will allow for $\sigma_s > 1$. By using a standardized framework, the arbitrary units are removed while the original σ/μ^* slope for the linearity analysis is retained (i.e., $\sigma/\mu^* = \sigma_s/\mu_s^*$), thereby facilitating better comparisons.

5) SELECTION OF OUTPUT VARIABLES

While the MOAT algorithm can identify significant factors, it can only determine the predictive power of a singular output value. Thus, a single number must be selected to represent the full spatial field of an output variable. Considering that haboobs are nonhomogeneous in space and time (Figs. 2–4) and often have a distinct head and wake region, this is nontrivial. After several tests, we selected the average of the cold pool surface layer, here taken to be the lowest model level (25 m AGL), split into 10-min intervals to retain the haboob's temporal progression. Originally, the haboob head and wake were identified separately and the analysis was run twice, but there was surprisingly little difference in factor importance. The same surface processes act on the head and the wake, thus allowing us to average over the full horizontal cold pool area. Surface values were selected to avoid the somewhat arbitrary process of identifying a haboob top. Shorter and longer temporal windows were tested, but 10-min intervals best capture the haboob's evolution without repeating data (Fig. S5).

4. Results

a. *Haboob characteristics*

Figures 2–4 demonstrate the evolution of a −16 K haboob in the first 30 min of the simulations for a daytime (Figs. 2 and 3) and nighttime (Fig. 4) case. As described in section 3a, the cold pool is released in the center of the domain and spreads radially outward (Fig. 2). The first 10 min of the simulations are generally associated with the dynamics of the cold bubble sinking and flattening out when it reaches the surface. It is only after this point that the land surface begins to feed back

onto the cold pool. The maximum wind and associated maximum in dust concentrations lie slightly behind the gust front boundary in the head region of the haboob, which has been noted elsewhere in observations (Marsham et al. 2013) and models (Huang et al. 2018). Due to weaker wind speeds in the trailing wake, less dust lofts in this portion of the cold pool and eventually begins to settle out gravitationally. Dust is confined to the low levels (Figs. 3 and 4g–i), with most vertical transport occurring in the haboob head, which reaches 1.2 km during the day and 1.0 km at night. The depth of the dust wake increases with time due to turbulent mixing and dust entering the wake from reverse flow in the head's overturning billows (Figs. 3 and 4j–l). Both the wake and head of the nighttime haboob are shallower than the daytime haboob due to the statically stable nocturnal boundary layer (Liu and Moncrieff 2000; Seigel and van den Heever 2012a).

Because of the hot and arid desert conditions, the cold pool weakens quickly due to surface fluxes and the entrainment of noncold pool air through Kelvin–Helmholtz waves at its upper boundary (Grant and van den Heever 2016; Knippertz et al. 2009). Nevertheless, because of the azimuthal averaging of the 3D simulations, the Kelvin–Helmholtz waves are not discernable in the 2D profiles. Dissipation occurs much faster in the daytime case than the nighttime case (Figs. 3 and 4a–c) owing to the strong, positive surface SHF. For most of the nighttime cases, SHF in the cold pool are negative and prevent dissipation. Due to the negative surface heat fluxes and stronger static stability, the nocturnal density currents propagate faster and farther before dissipating and produce stronger vertical velocities at the gust front than the daytime density currents. This is consistent with Bukowski and van den Heever (2021), who noted a similar increase in nocturnal haboob strength in simulations using the Weather Research and Forecasting Model coupled to Chemistry (WRF-Chem), showing a robust response across models.

b. *Sensitivity analysis*

The MOAT sensitivity analysis allows us to determine how important an input factor is to a modeled output value. To fully understand dust uplift, it is also necessary to predict which factors are important for the parent cold pool. Thus, in this section we will consider which surface parameters are significant predictors of cold pool temperature/wind speed, surface heat fluxes, and last, dust concentrations.

1) COLD POOL TEMPERATURE

In predicting surface cold pool temperature (Figs. 6a,b), the initial cold pool temperature is the most important factor at the beginning of the simulations, a result that is expected and demonstrates that the MOAT algorithm is functioning properly. However, the effect of the initial cold pool temperature fades beyond the first 10–20 min, once the cold pool has descended and land surface interactions have had an opportunity to modify the density current, eventually being replaced by surface type (desert, semidesert, short grassland, crop–grassland) as the most significant factor. The underlying surface type affects variables such as albedo, heat fluxes and momentum transfer, and evapotranspiration, all of which control cold pool dissipation and strength, especially as the haboob ages. Soil moisture and soil type are less significant (yet still influential) for predicting daytime cold pool temperature and winds [via Eq. (3)]. While the thermal soil characteristics (soil type) and soil water content also contribute to the partitioning of sensible and latent heat fluxes, they are both ranked lower than surface type in this regard. Because SHFs are negative at night, the segmentation between SHFs and LHFs has much less of an effect on cold pool strength, meaning soil type and moisture have only minor effects on nocturnal haboob intensity. Although surface type remains important at night, it is more likely because of roughness length effects on momentum transfer rather than heat flux portioning.

The interacting combination of factors responsible for partitioning surface fluxes during the day versus night is evident in the nonlinearity analysis in Figs. 6c and 6d as indicated by the location of points relative to the MOAT (σ_s–μ_s^*) plane (Fig. 5b). The daytime interactions across input variables are much stronger and nonlinear, while the nonlinearity decreases at night. Thus, there are fewer complex land surface interactions affecting cold pool strength at night. Overall, surface type stands out as a critical, yet highly nonlinear factor for predicting haboob temperature and wind speed during both day and night.

2) SURFACE HEAT FLUXES

Although the initial cold pool strength is significant for predicting haboob temperature and therefore horizontal wind speed, it is less important for forecasting surface heat fluxes (Fig. 7). Despite the wind velocity component in the surface flux equations [Eq. (2)], initial cold pool strength is relatively insignificant. This implies that surface heat fluxes in a desert cold pool are more sensitive to variations in the roughness length or the moisture/temperature gradient than they are to changes in the wind speed. Even though the initial cold pool temperature is essentially unimportant during the day, SHFs depend more on cold pool temperature during the night, along with surface type. Since cold pool evolution and dissipation depends strongly on SHFs, it is unsurprising that these two output variables (cold pool temperature and SHF) are related and share similar responses and factor ranks.

Generally, the land surface interactions required to predict LHFs (Figs. 8c,d) are more complicated and nonlinear than those for SHFs (Figs. 7c,d). Similarly, initial cold pool temperature is unimportant during the day compared to surface type, but now the soil type and soil moisture also play a role in the LHFs. Physically, because LHF depends on the moisture gradient between the air and the surface, initial soil moisture and the inherent moisture retaining properties of each soil type will be essential. Soil thermal properties are also relevant for flux partitioning and seem to be crucial in the nighttime LHF case, where soil clay content is ranked as the principal factor.

3) DUST CONCENTRATION

Because cold pool temperature drives horizontal winds and dust emissions are proportional to wind speed, the fact that

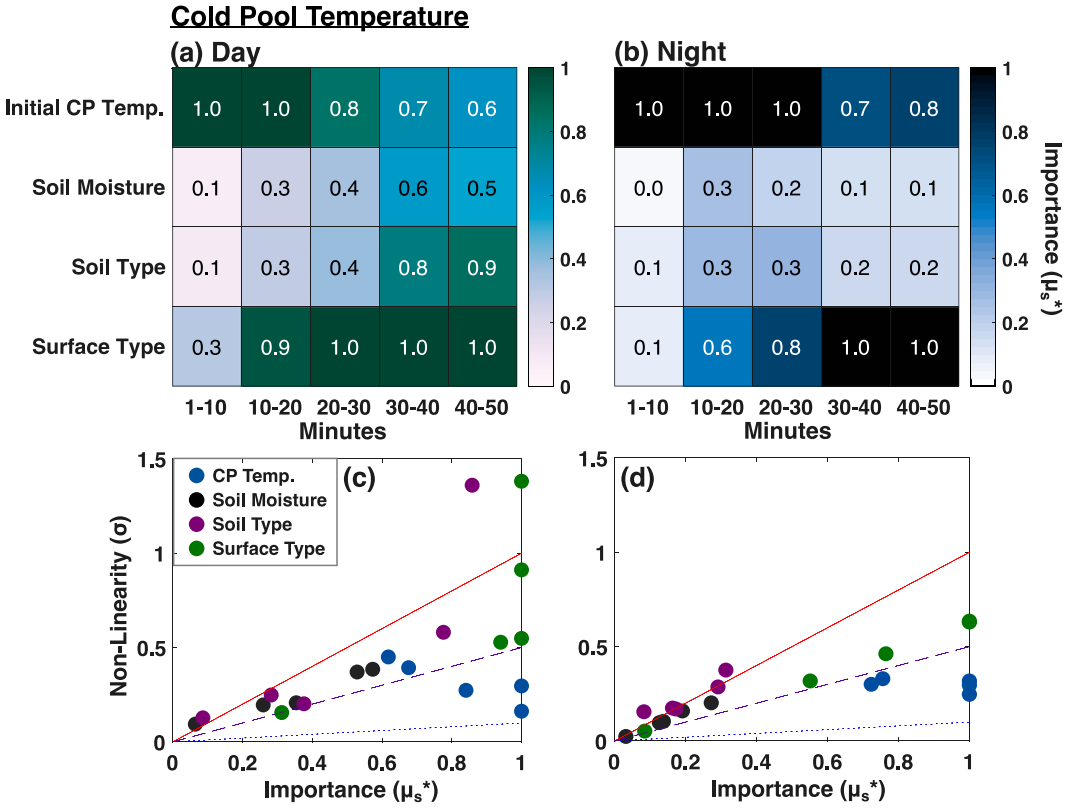

FIG. 6. (a),(b) Heat map time series of μ_s^* values ranging from 0 (unimportant) to 1 (most important) in predicting surface cold pool temperature for the (a) daytime and (b) nighttime cases. The four rows in each panel represent the four input parameters (initial cold pool temperature, soil moisture, soil type/clay fraction, and surface type), while the abscissa is simulation time after initialization, split into 10-min averages. (c),(d) The Morris σ_s–μ_s^* plane (as demonstrated in Fig. 5) for the corresponding heat map above it. Each of the four input parameters (cold pool temperature: blue; soil moisture: black; soil type: purple; surface type: green) has five data points that correspond to the five separate 10-min windows in (a) and (b). There is no significance to the difference in color scheme between day and night in (a) and (b); it exists only to distinguish the two from each other.

dust concentrations are most dependent on cold pool temperature was expected (Fig. 9). In terms of land surface parameters, the second most important parameter for predicting dust concentrations is again surface type, which is followed by soil type and finally soil moisture. Despite the dust parameterization including a scaling factor for moisture [Eq. (1)], it seems to have little effect on dust concentrations because the scaling factor in Eq. (1) only operates across a small range of soil moistures. For our experimental haboob case, soil moisture may matter more due to its effect on LHF than because of the dust emission scaling term, but it is relatively unimportant in both scenarios. Soil type is more important than soil moisture, and its effect is enhanced at night, possibly from the effect that soil type has on moisture and thermal heat retention.

In the nonlinearity plots, soil type and surface type exhibit either highly nonlinear behavior or an interaction between these two variables (Figs. 9c,d). As a result, understanding the physical mechanisms behind these factors is challenging. Soil type can have a nonmonotonic relationship to dust concentrations in that more clay content does not always correspond to more dust. A hypothesis for this nonmonotonic behavior related to the intrinsic properties of soil types can be found in section 4c(3). Although the surface parameters exhibit nonlinearity, the initial cold pool temperature is only slightly nonlinear in its relationship to haboob dust during both day and night (Figs. 9c,d). Based on where the cold pool temperature lies on the σ_s–μ_s^* plane, the relationship between cold pool temperature and haboob dust emissions must be higher than a first-degree linear polynomial, but lower than a quadratic or higher-degree polynomial, even though dust emissions scale as U^2 to U^3. We hypothesize that a relatively simple theoretical formulation could explain this relationship unearthed in the sensitivity analysis.

First, reducing Eq. (1) by removing the scaling factor E_{Z_0}, the bin partitioning term (s_p), and the soil moisture correction ($\mathrm{Ut}_{\mathrm{wet}}$), which was consistently ranked the lowest factor of importance in this analysis, produces Eq. (4), which relates dust flux, F, to the third power of near-surface wind U. The cold pool intensity (V^2) can also be substituted from Eq. (3):

$$F \propto U^3 \propto V^3 \propto (V^2)^{3/2}. \tag{4}$$

Expanding Eq. (4) using the full form of Eq. (3) gives

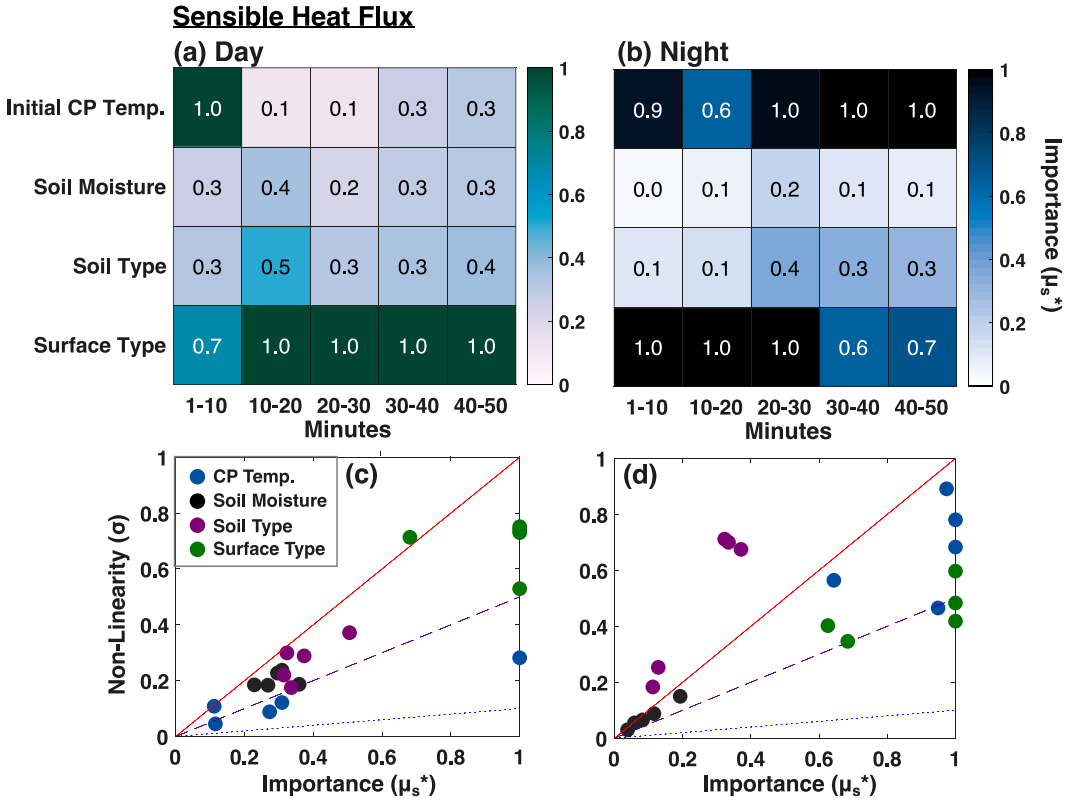

FIG. 7. As in Fig. 6, but for sensible heat flux.

$$F \propto \left(2\int_0^H - g\frac{\theta'}{\overline{\theta}_{\text{env}}}\,dz\right)^{3/2}. \tag{5}$$

Equation (5) can be simplified into the proportionality statement in Eq. (6) that, to first order, relates dust flux (F) to the cold pool perturbation potential temperature (θ') relative to its environment ($\overline{\theta}_{\text{env}}$):

$$F \propto \left(\frac{\theta'}{\overline{\theta}_{\text{env}}}\right)^{3/2}. \tag{6}$$

In this relationship, dust flux is proportional to cold pool temperature and is within the range of exponents (~1–2) expected from the linearity analysis (Figs. 8c,d). There is a clear relationship between dust emissions in an outflow boundary and the temperature of the density current. This relationship suggests that dust emissions can be predicted or based primarily on cold pool temperatures, although more testing is necessary.

c. *Physical mechanisms*

The MOAT sensitivity analysis identified the most important surface factors for predicting haboob temperature, dust, and surface heat fluxes. Nevertheless, MOAT can only distinguish significant factors from insignificant ones and cannot explain *why* these factors are important or ascertain which underlying physical mechanisms are responsible for the effect. While the MOAT sampling strategy does not test all combinations of input factors, there are a limited number of trajectory combinations that perturb only one input factor and hold all others constant. Using this subsample of perturbed simulations allows for a more traditional one-at-a-time factor analysis, whereby processes can be examined and attributed. Within the 120 simulations, 24 (12 days and 12 nights) exist in the subsample that represent three factors (soil moisture, soil type, and land surface type) with four value perturbations each. Although the traditional one-at-a-time analysis is useful for understanding the mechanisms, it is important to note that the full sensitivity and nonlinearity cannot be established with this method. The exact combination of factors may be critical and can introduce nonmonotonic behavior, hence the need for more sophisticated sensitivity algorithms.

1) DAY VERSUS NIGHT

The nighttime simulations include fewer complex interactions due to reduced or negative SHFs and will only be discussed for the soil moisture case, but plots for nighttime soil and surface type are included in the supplementary materials (Figs. S2 and S3). The trends are similar across input factors and are analogous to the conclusions in section 4a and Figs. 2–4: nighttime haboobs are stronger, shallower, and longer lasting. This is because of (i) negative SHFs and (ii) a nocturnal surface inversion formed in a more statically stable boundary layer that

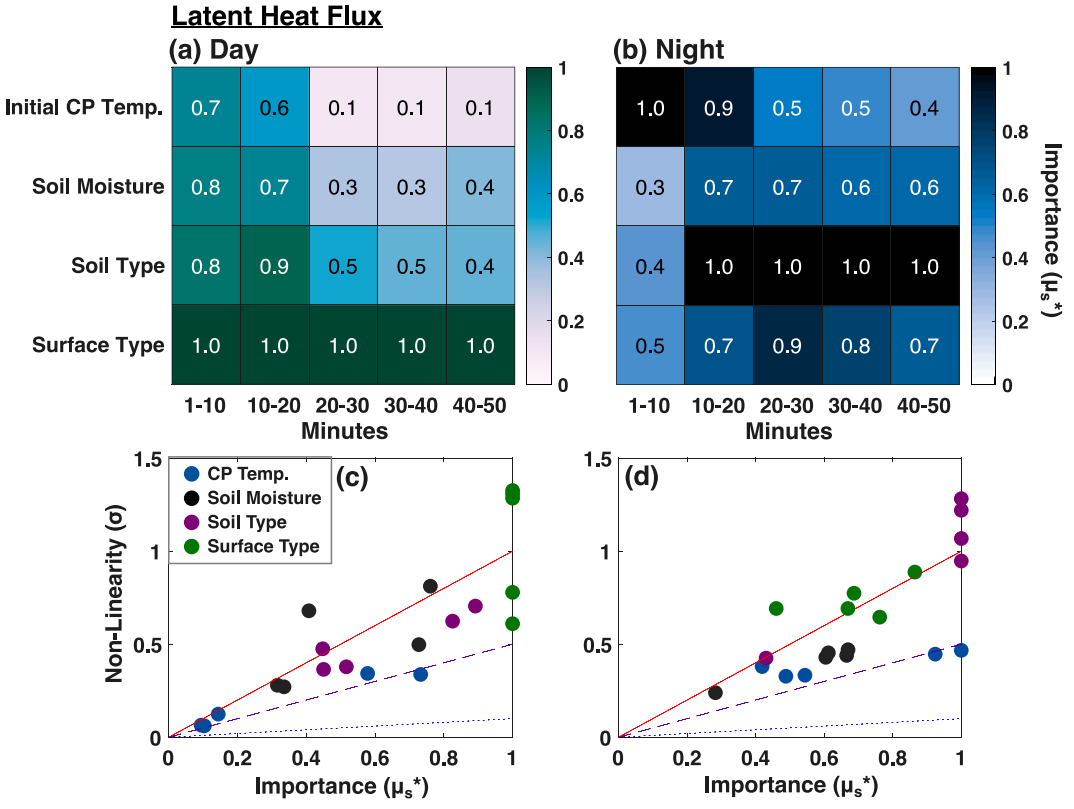

FIG. 8. As in Fig. 6, but for latent heat flux.

enhances density current intensity (Liu and Moncrieff 2000; Seigel and van den Heever 2012a). These stronger cold pools loft more dust throughout their extended lifetime, and the vertical extent of mixing is suppressed by the nocturnal inversion. These processes all lead to longer periods of increased dust concentrations in nocturnal haboobs, especially near the surface.

2) SOIL MOISTURE

In the MOAT factor analysis, soil moisture was consistently ranked as the least important, yet most linear factor in its impact on the haboob processes of interest. In Fig. 10, the initial dynamic sinking and spreading out of the cold pool is evident in a strong perturbation in the first 10 min, followed by the much slower land feedbacks and dissipation mechanisms over the remaining hour of simulation time. Nonetheless, soil moisture still has an effect as the haboob progresses, whereby increasing soil moisture leads to lower dust concentrations in the haboob (Figs. 10a,b) for both the day and night cases. From observational studies, it has been shown that moister soils impede lofting by increasing soil cohesion, which is accounted for in Eq. (1) and scales emissions accordingly.

Still, interactions within the cold pool can also contribute to the observed differences in dust concentration. During the daytime, LHFs increase as soil moisture increases (Figs. 10g,h) because energy is evaporating soil water, cooling the cold pool (Figs. 10c,d), and preventing energy from heating the surface, consequently reducing SHFs (Figs. 10e,f). In an opposing effect, colder cold pools should lead to stronger winds via Eq. (3) and enhance dust uplift. One hypothesis may be that as SHFs are reduced in the moist soil scenario, there is less mixing and less dissipation of the density current, which results in the cold pool propagating faster across the domain thereby lofting more dust in the process. A second complicating factor is that a decrease in SHF leads to less downward momentum transport, which diminishes the near-surface wind speed and reduces dust emissions (Foroutan et al. 2017; Huang et al. 2018). A third possibility is that the effect of the soil moisture scaling factor in the dust parameterization, which represents dust suppression due to wet soil cohesion forces, is more significant than feedbacks between LHF, evaporation, and cooling inside the cold pool. Most likely, all three of these proposed mechanisms are operating concurrently.

Interestingly, the moist soil density currents propagate farther during the daytime (not shown) than their dry soil counterparts because the SHFs dissipate the dry soil cold pools faster. Despite the density currents being longer lived in moister conditions, the wind speed near the end of their lifetime is weak and lofts significantly less dust than at the beginning of the simulation when the cold pools are intense and exhibit strong wind speeds. Nevertheless, the extended lifetime of dust lofting in the moist-soil case cannot overcome and replace the soil moisture-induced dust deficit from the beginning of the haboob's lifetime (Fig. 10a).

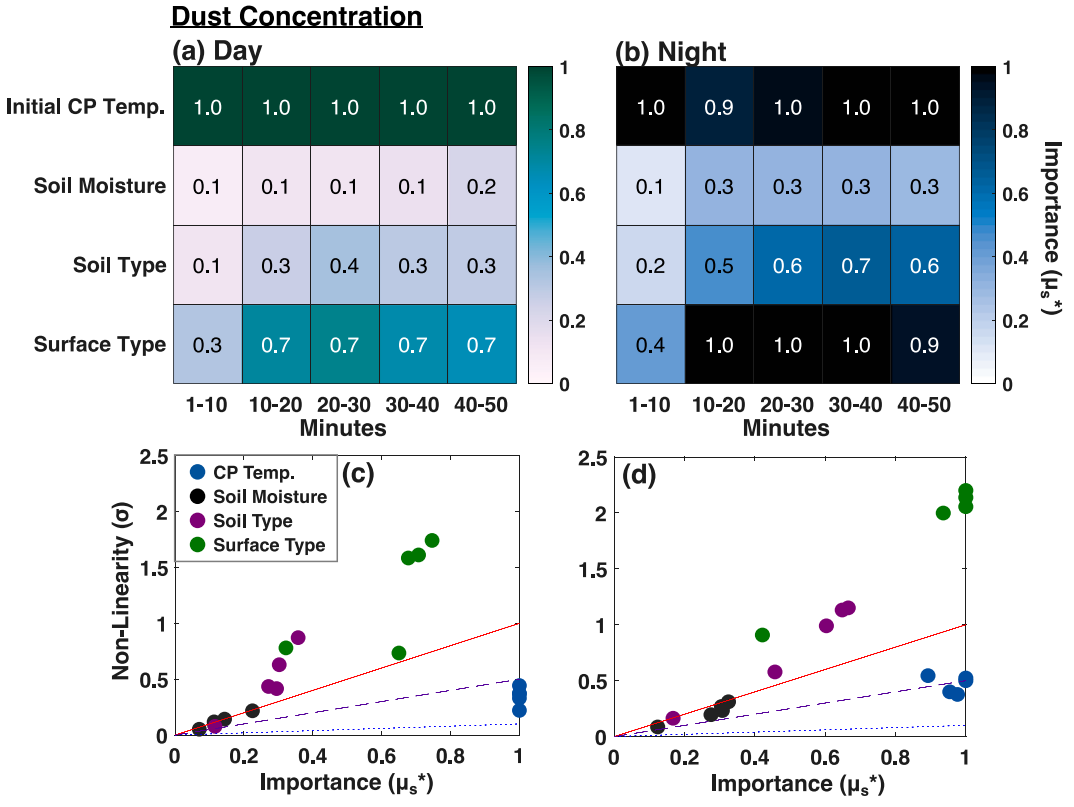

FIG. 9. As in Fig. 6, but for surface dust concentrations.

In the nighttime case, there is again more dust in the dry soil haboobs (Fig. 10b) and higher surface concentrations of dust compared to the daytime case, but little change to the cold pool temperature (Fig. 10d). SHFs (Fig. 10f) do not change due to soil moisture at night because the surface is no longer absorbing incoming solar radiation and has cooled faster than the air above it. In fact, the surface is colder than the cold pool air, which is evident by the SHFs being negative. Additionally, LHFs at night are also negative, denoting that the surface is drier than the cold pool (Fig. 10h). Negative SHFs prevent the cold pool from dissipating and are almost identical across the different soil moisture values, thus having little to no effect on temperature, momentum transfer, or wind speed. As such, the difference in dust concentrations must come from the soil moisture scaling factor in the dust emission equation [(Eq. (1)] for the nighttime case.

3) SOIL TYPE AND CLAY FRACTION

Soil type was identified by the MOAT sensitivity analysis to be the second most important factor in influencing cold pool temperature and haboob dust, demonstrating nonlinear and nonmonotonic behavior. From laboratory studies (Fécan et al. 1999), it has been shown that soils with high clay fractions will loft more dust than low clay fraction soils at the same soil moisture [Eq. (1)]. However, the nonmonotonic nature of the soil type response discovered in section 4b indicates that increasing clay fraction does not always result in an increase in dust emissions and suggests that it interacts with other input parameters. Indeed, while the nighttime haboob follows the theory that high clay fractions will loft more dust (Fig. S2), later in the simulation the 40% clay fraction simulation has higher dust concentrations than the 48% clay simulation, as does the 57% versus the 65% clay soil (Fig. 11a).

Integral to the understanding of this nonmonotonic response is the fact that changing the soil type inadvertently changes other soil properties. Soil textures are classified by their relative percentage of clay, sand, and silt particles, with loam-type soils exhibiting a balanced mix of the three component textures. Since the total clay/sand/silt composition must equal 100%, a decrease in the amount of clay must be matched by an increase in silt or sand. The difference in soil texture leads to differences in other parameters such as porosity, water retention, and thermal conductivity, but it does not significantly alter the albedo or roughness length in this study. Clay and clay loam soils have lower thermal conductivities, which means less energy will go into the ground and more will be transferred to the atmosphere via SHFs (Fig. 11c) (Rempel and Rempel 2016), increasing the near-surface temperature compared to soils that contain silt. Clay and clay loam soils also evaporate less and retain more water than silty soils (Rempel and Rempel 2016). When soil retains water rather than evaporating it, LHFs are reduced (Fig. 11d), which prevents evaporative cooling of the cold pool. Therefore, clay soil has not only the highest SHFs and warmest cold pool, but also the weakest wind speeds and lower dust emissions. Here, there is likely an increase in

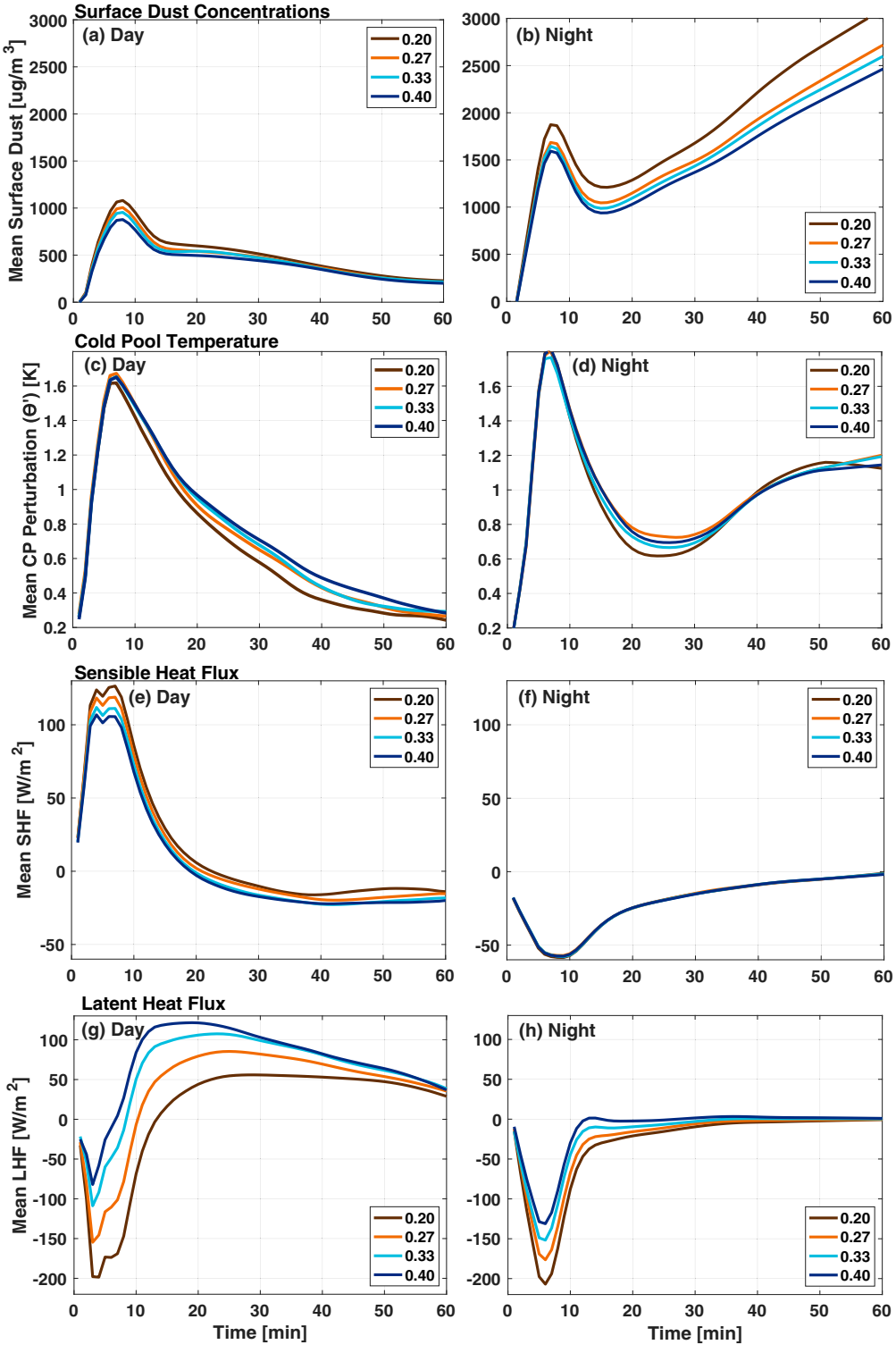

FIG. 10. Time series representing the effect of initial soil moisture on the horizontal mean across the whole cold pool for (a),(b) surface dust concentrations, (c),(d) absolute value cold pool temperature perturbation, (e),(f) sensible heat flux, and (g),(h) latent heat flux for (left) day and (right) night. The colored lines represent 20% soil saturation (dark brown), 27% (light brown), 33% (light blue), and 40% (dark blue) initial soil moisture. The simulations were all initialized with a −16.66 K cold pool, silty loam soil, and a short grassland surface and are identical besides the initial soil moisture.

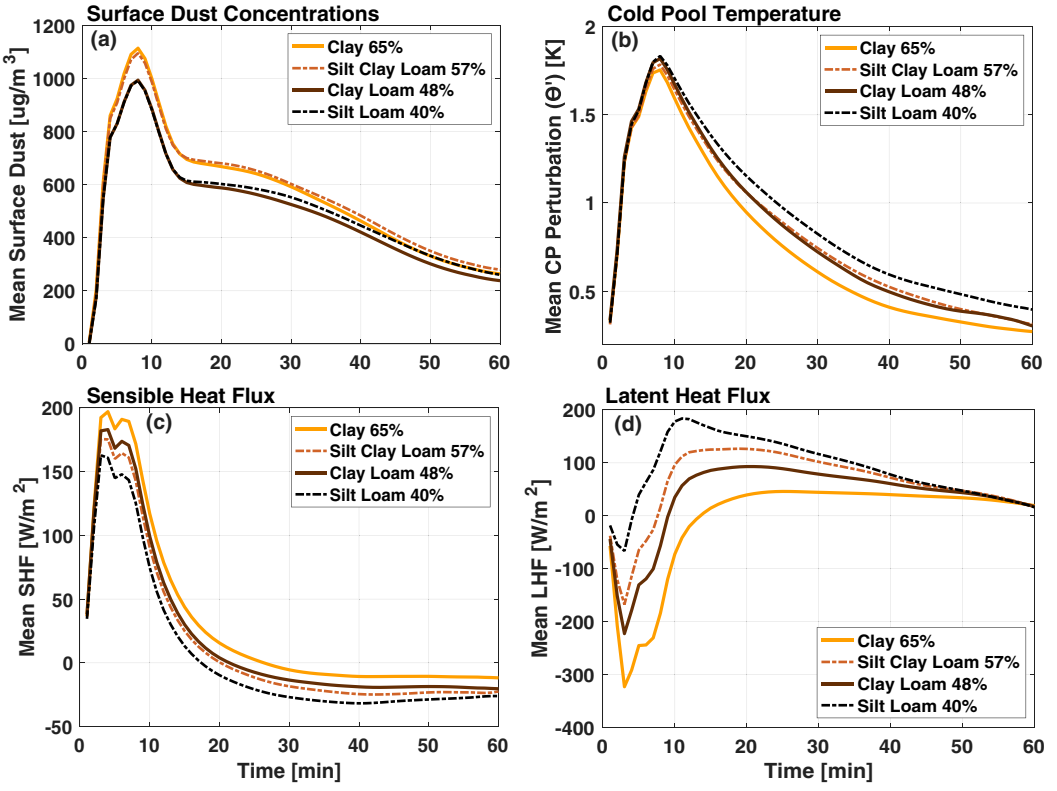

FIG. 11. As in Fig. 10, but for soil type during the day only. The lines represent clay (65%—yellow), silty clay loam (57%—orange), clay loam (48%—dark brown), and silty loam (40%—black) soils. Silty soils are indicated by hatching. The simulations were all initialized with a −13.33 K cold pool, 33% soil moisture, and a cropland surface and are identical besides the initial soil type.

downward momentum transfer due to SHFs, but it does not compensate for the silty soils producing a colder density current.

Returning to the nonlinearity analysis, there are two competing factors in the daytime haboob: the increase in dust emissions as clay fraction increases, versus silty soils producing colder and stronger cold pools due to higher LHFs. The balance of these complex and competing processes leads to nonmonotonic results and has implications for modeling dust emissions in haboobs, namely, that the clay/sand/silt composition matters for surface fluxes *and* the interaction between the cold pool and the land surface. The USDA soil taxonomy classifies 12 different soil mixtures (Soil Survey Staff 1999), each of which could elicit a different response to cold pools and dust emissions based on their thermal and moisture properties and the environment.

4) LAND SURFACE TYPE

Besides the initial cold pool temperature, surface type was identified as the most important factor for predicting haboob dust concentrations and intensity. Like soil type, it exhibited nonlinear and nonmonotonic behavior in that moving from a desert to a more vegetated surface type does not necessarily decrease dust amounts. Because dust mobilization is inhibited as roughness length increases, this surface effect is represented in the dust parameterization through a roughness length scaling factor [(Eq. (1)]. Complicating matters, surface heat fluxes are also scaled by roughness length through the drag coefficient in Eq. (2), in which smaller roughness lengths decrease the drag coefficient and hence decrease the magnitude of the heat fluxes. Furthermore, there are higher-order effects of the surface layer, such as surface albedo, that impact dust emissions via physical interactions with the cold pool but are not investigated here.

In both the day and night, dust concentrations closely follow the trend of the roughness scaling factor. The bare soil desert and grassland surfaces have the lowest vegetation heights and therefore the lowest roughness lengths of the land types tested in this experiment (Fig. 12f). Because they lack a tall vegetation shield and turbulent momentum can reach the surface, dust can loft freely in the desert and grassland (Fig. 12a). Conversely, the simulations with higher vegetation heights, such as the agricultural land surface and semideserts with tall shrubs and cacti, exhibit less dust lofting. The effect of roughness length on dust emissions can be substantial. For instance, the desert land type has the highest dust concentrations, despite exhibiting a weaker cold pool (Fig. 12c), lower outflow wind speeds, and suppressed heat fluxes (Fig. 12d). This apparent contradiction arises because the increase in dust due to the shorter roughness length clearly dominates

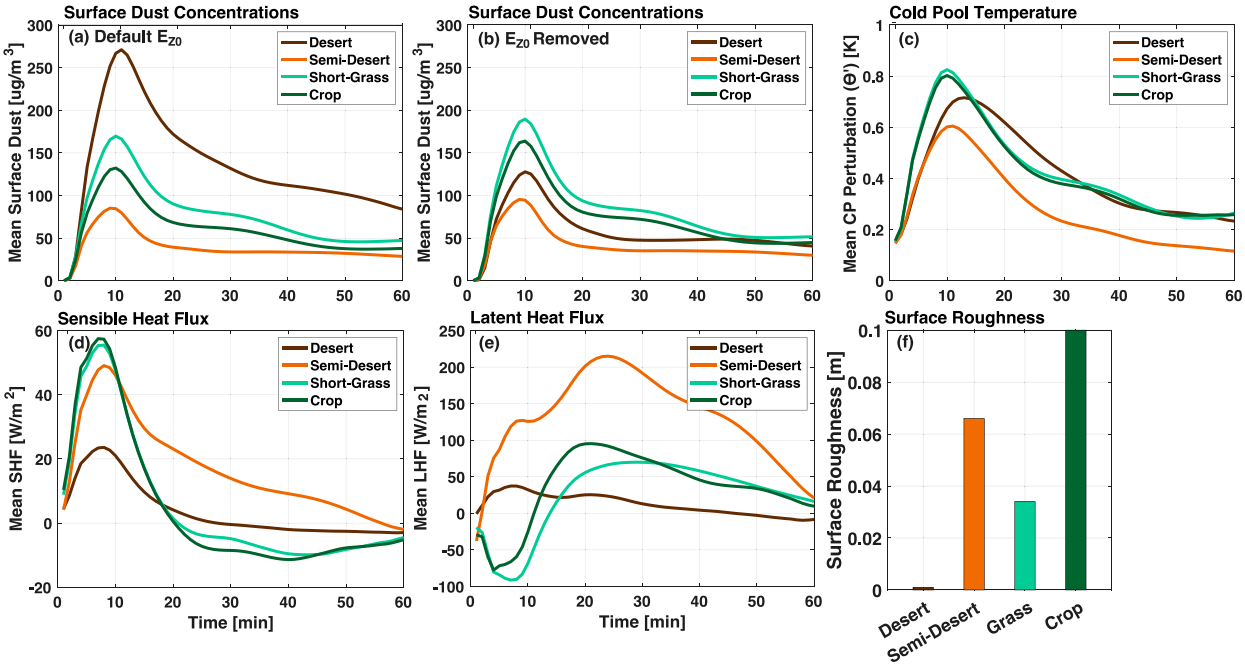

FIG. 12. As in Fig. 10, but for the four different surface types during the day only. The colors represent desert (dark brown), semidesert (orange), grassland (light green), and cropland (dark green). The simulations were all initialized with a −10 K cold pool, 40% soil moisture, silty clay loam soil and are identical besides the surface type. (a) The original simulations including the roughness length scaling factor in Eq. (1) (E_{Z_0}) [and shown in (f)], (b) this scaling factor has been removed in the dust parameterization, and (c)–(e) the scaling factor was not removed for any of the other panels.

over all other feedbacks in the system. However, the roughness length effect on heat fluxes and haboob evolution is also evident. For instance, the semidesert surface has the weakest cold pool but strong surface fluxes because it includes tall vegetation that increases momentum transport [Eq. (2)], whereas the desert has a vanishingly small roughness length that leads to suppressed surface fluxes.

Because the roughness length impacts both dust and heat fluxes simultaneously, it is almost impossible to deconvolve the summation of effects and isolate the vegetation effects outside of the roughness parameter. As a first step, these four one-at-a-time simulations were rerun with the roughness length scaling factor removed in the dust parameterization but retained in the heat flux equations. As such, this modification only affects dust uplift and not surface feedbacks to the density current. The result shows a more straightforward, monotonic relationship in agreement with the theory that more intense cold pools loft more dust (Fig. 12b).

It is therefore imperative that we find skillful means of representing vegetation height in dust models to accurately predict emissions and land surface feedbacks. While high-resolution land-cover data are available, translating complicated, heterogeneous landscapes with numerous sources of roughness into a single characteristic value in numerical models is nontrivial. Additionally, land surface models like LEAF-3 are often categorical and combine roughness height with vegetation land coverage and interactions (e.g., albedo, transpiration) which also go on to affect surface fluxes. Selecting the correct roughness length or vegetation cover may therefore come at the expense of degrading other surface variables, or a truly accurate combination may simply not exist. There are similar concerns related to determining an accurate representation of roughness length scaling factors in dust mobilization parameterizations. Despite the significance of the roughness scaling factor, it is not included in all dust parameterizations. It is a highly sensitive parameter that modulates dust emissions comprehensively and cannot be set, included, or dismissed arbitrarily.

5. Conclusions

In this study we conducted a suite of 120 idealized model simulations of daytime and nighttime haboobs to better understand feedbacks between dust producing cold pools and their underlying surface. The simulations covered a wide range of initial parameters, including varied initial cold pool temperatures, surface type, soil moisture, and soil type, based on previous work showing the importance of these factors for both dust mobilization *and* cold pool dynamics. The ensemble of simulations was analyzed with the Morris one-at-a-time (MOAT) sensitivity method to identify which of the input surface parameters are most significant in predicting haboob temperature, surface fluxes, and dust uplift. Single simulations were then utilized in a traditional one-at-a-time analysis to understand why these factors are significant or insignificant

and to attribute physical mechanisms to the understanding of haboob physics.

The MOAT sensitivity analysis ranked the most important input factors for predicting haboob dust concentrations and properties as 1) initial cold pool temperature, 2) surface type (desert, semidesert, short grassland, agricultural cropland), 3) soil type/clay content (clay/65%, silt clay loam/57%, clay loam/48%, and silt loam/40%), and 4) soil moisture saturation fraction (0.20, 0.27, 0.33, and 0.40).

First, the initial cold pool temperature is the most significant parameter because cold pool temperature drives wind speeds, which drive dust emissions. Initial cold pool strength is important for the entire lifetime of nocturnal haboobs, but is important only at the beginning of the haboob's lifetime for daytime cases. In the day, the impact of the initial cold pool temperature is offset by positive SHFs which warm and dissipate the cold pool, but also increase gustiness and dust uplift due to the enhanced downward transport of momentum. Conversely, negative heat fluxes at night strengthen the cold pools, leading to nocturnal haboobs being stronger in terms of dust uplift, propagation distance, and speed.

Surface type was identified as the second most important factor for predicting haboob properties, and the effects are dominated by roughness length. Increased roughness length decreases dust emissions such that bare soil deserts loft more dust than surfaces with tall vegetation, such as semideserts or cropland. However, higher roughness lengths also increase heat fluxes, which can enhance wind speeds and dust uplift. Running tests with the roughness length scaling factor removed in the dust parameterization demonstrated that the roughness length has an outsized impact on dust concentrations compared to all other feedbacks. Soil type follows surface type in importance, and it generally supports the theory that a higher clay fraction of soil is associated with more dust lofting. But differences in thermal conductivity and moisture retention in clay versus silty soils have an effect in daytime haboobs due to the partitioning of sensible versus latent heat fluxes.

Soil moisture was consistently ranked as the least important parameter for predicting haboob dust, despite the soil moisture scaling factor in the dust parameterization that represents moist soil cohesion forces. However, the range of soil moistures tested in the ensemble represent a dry environment conducive for dust emissions and are not moist enough to completely prohibit dust lofting. Soil moisture is ranked last only in terms of its role as a modulating land surface factor in dry dust-producing conditions. In this regard, it was observed that moist-soil haboobs propagate farther during the day because of the reduced SHF compared to dry-soil haboobs. However, moist-soil haboobs display relatively weaker wind speeds in the beginning of their lifetime, therefore lofting less dust overall compared to dry-soil cold pools. This effect may be modulated by cold pool life cycle and may not be applicable to long-lived cold pools.

Finally, a semilinear relationship between haboob dust concentrations and cold pool temperature was observed in the sensitivity analysis and was independent of the time of day. By combining the dust flux parameterization with the cold pool intensity equation, a relationship between dust flux and cold pool temperature was derived. This relationship provides an opportunity to relate haboob dust uplift to the thermodynamic environment and cold pool strength, and has the potential to reduce online calculations, improve statistical representations of dust emissions, and simplify the framework of dust–cold pool interactions.

The sensitivity analysis presented here has provided insight into which parameters are most important for modeling dust emissions in convective outflow boundaries. Most important is modeling the correct cold pool temperature, which is challenging because of the complicated microphysical–dynamical–environmental feedbacks in convective downdrafts. An accurate roughness length is also crucial for predicting dust emissions and haboob propagation because it impacts both dust emission and surface fluxes. Soil moisture is generally unimportant, which agrees with previous literature suggesting erodible topsoil dries quickly in arid regions and may not be a significant parameter in practice. It is important to note that while soil moisture effects may play a minor role in the dissipation and dust emissions of dryland haboobs, this result should not be extended to cold pools more generally. Soil moisture can impact the initiation of convection and initial cold pool strength, and moisture feedbacks may be important in more moist or tropical environments.

However, remaining challenges mean that future work is necessary. One limitation of this study is that it tests only one model with a single dust parameterization. While parameterizations are designed to represent physical processes, dust modeling is complicated by differences in how to approach this representation and by using multiple scaling factors in the formulas. It would be illuminating to reproduce this project with varying dust prediction methods to compare the sensitivities across parameterizations. Further limitations include the modeled environment only responding to the land surface for the 4 h of simulation time and the use of a single sounding for the initial conditions. The higher-order effects of environment–surface correlations should be tested under varying environmental conditions, but this is left for future work. Namely, experiments representing more environments with dust-lofting ecosystems, such as dry grasslands, will help expand this knowledge. Furthermore, studies considering long-lived haboobs that will emit substantially more dust than the isolated convective outflows in this study are also necessary for better understanding and prediction of long-lived haboobs. Even though more scenarios need to be tested, much has been learned regarding which land surface factors are most important for modeling and forecasting haboobs, alongside the physical mechanisms and feedbacks between cold pools, the land surface, and dust mobilization.

Acknowledgments. This work was funded by an Office of Naval Research–Multidisciplinary University Research Initiative (ONR-MURI) grant (N00014-16-1-2040).

Data availability statement. The namelists required to reproduce the RAMS simulations and links to all open source code

and public datasets used in this study are stored at the following repository: https://doi.org/10.5061/dryad.6hdr7sr4d.

REFERENCES

Abu-Hamdeh, N., 2003: Thermal properties of soils as affected by density and water content. *Biosyst. Eng.*, **86**, 97–102, https://doi.org/10.1016/S1537-5110(03)00112-0.

Alfaro, S. C., and L. Gomes, 2001: Modeling mineral aerosol production by wind erosion: Emission intensities and aerosol size distributions in source areas. *J. Geophys. Res.*, **106**, 18 075–18 084, https://doi.org/10.1029/2000JD900399.

Baddock, M. C., C. L. Strong, P. S. Murray, and G. H. McTainsh, 2013: Aeolian dust as a transport hazard. *Atmos. Environ.*, **71**, 7–14, https://doi.org/10.1016/j.atmosenv.2013.01.042.

Baron, P. A., and K. Willeke, 2001: *Aerosol Measurement: Principles, Techniques and Applications*. 2nd ed. Wiley-Blackwell, 1160 pp.

Bell, J. E., and Coauthors, 2018: Changes in extreme events and the potential impacts on human health. *J. Air Waste Manage. Assoc.*, **68**, 265–287, https://doi.org/10.1080/10962247.2017.1401017.

Belnap, J., S. L. Phillips, and M. E. Miller, 2004: Response of desert biological soil crusts to alterations in precipitation frequency. *Oecologia*, **141**, 306–316, https://doi.org/10.1007/s00442-003-1438-6.

Benjamin, T. B., 1968: Gravity currents and related phenomena. *J. Fluid Mech.*, **31**, 209–248, https://doi.org/10.1017/S0022112068000133.

Bergametti, G., J. L. Rajot, C. Pierre, C. Bouet, and B. Marticorena, 2016: How long does precipitation inhibit wind erosion in the Sahel? *Geophys. Res. Lett.*, **43**, 6643–6649, https://doi.org/10.1002/2016GL069324.

——, and Coauthors, 2017: Dust uplift potential in the central Sahel: An analysis based on 10 years of meteorological measurements at high temporal resolution. *J. Geophys. Res. Atmos.*, **122**, 12 433–12 448, https://doi.org/10.1002/2017JD027471.

Bishop, J. K. B., R. E. Davis, and J. T. Sherman, 2002: Robotic observations of dust storm enhancement of carbon biomass in the North Pacific. *Science*, **298**, 817–821, https://doi.org/10.1126/science.1074961.

Boose, Y., and Coauthors, 2016: Heterogeneous ice nucleation on dust particles sourced from nine deserts worldwide—Part 1: Immersion freezing. *Atmos. Chem. Phys.*, **16**, 15 075–15 095, https://doi.org/10.5194/acp-16-15075-2016.

Bou Karam, D., C. Flamant, P. Tulet, J.-P. Chaboureau, A. Dabas, and M. C. Todd, 2009: Estimate of Sahelian dust emissions in the intertropical discontinuity region of the West African monsoon. *J. Geophys. Res.*, **114**, D13106, https://doi.org/10.1029/2008JD011444.

——, E. Williams, M. Janiga, C. Flamant, M. McGraw-Herdeg, J. Cuesta, A. Auby, and C. Thorncroft, 2014: Synoptic-scale dust emissions over the Sahara Desert initiated by a moist convective cold pool in early August 2006. *Quart. J. Roy. Meteor. Soc.*, **140**, 2591–2607, https://doi.org/10.1002/qj.2326.

Brahney, J., A. P. Ballantyne, C. Sievers, and J. C. Neff, 2013: Increasing Ca^{2+} deposition in the western US: The role of mineral aerosols. *Aeolian Res.*, **10**, 77–87, https://doi.org/10.1016/j.aeolia.2013.04.003.

Bryan, G. H., and R. Rotunno, 2014: Gravity currents in confined channels with environmental shear. *J. Atmos. Sci.*, **71**, 1121–1142, https://doi.org/10.1175/JAS-D-13-0157.1.

——, J. C. Wyngaard, and J. M. Fritsch, 2003: Resolution requirements for the simulation of deep moist convection. *Mon. Wea. Rev.*, **131**, 2394–2416, https://doi.org/10.1175/1520-0493(2003)131<2394:RRFTSO>2.0.CO;2.

Bukowski, J., and S. C. van den Heever, 2020: Convective distribution of dust over the Arabian Peninsula: The impact of model resolution. *Atmos. Chem. Phys.*, **20**, 2967–2986, https://doi.org/10.5194/acp-20-2967-2020.

——, and ——, 2021: Direct radiative effects in haboobs. *J. Geophys. Res. Atmos.*, **126**, e2021JD034814, https://doi.org/10.1029/2021JD034814.

Burrell, A. L., J. P. Evans, and M. G. De Kauwe, 2020: Anthropogenic climate change has driven over 5 million km^2 of drylands towards desertification. *Nat. Commun.*, **11**, 3853, https://doi.org/10.1038/s41467-020-17710-7.

C3S, 2017: ERA5: Fifth generation of ECMWF atmospheric reanalyses of the global climate. Copernicus Climate Change Service CDS, accessed 26 September 2020, https://cds.climate.copernicus.eu/cdsapp#!/home.

Campolongo, F., J. Cariboni, and A. Saltelli, 2007: An effective screening design for sensitivity analysis of large models. *Environ. Modell. Software*, **22**, 1509–1518, https://doi.org/10.1016/j.envsoft.2006.10.004.

Cantero, M. I., S. Balachandar, M. H. García, and D. Bock, 2008: Turbulent structures in planar gravity currents and their influence on the flow dynamics. *J. Geophys. Res.*, **113**, C08018, https://doi.org/10.1029/2007JC004645.

Cotton, W. R., and Coauthors, 2003: RAMS 2001: Current status and future directions. *Meteor. Atmos. Phys.*, **82**, 5–29, https://doi.org/10.1007/s00703-001-0584-9.

Covey, C., D. D. Lucas, J. Tannahill, X. Garaizar, and R. Klein, 2013: Efficient screening of climate model sensitivity to a large number of perturbed input parameters. *J. Adv. Model. Earth Syst.*, **5**, 598–610, https://doi.org/10.1002/jame.20040.

Cowie, S. M., J. H. Marsham, and P. Knippertz, 2015: The importance of rare, high-wind events for dust uplift in northern Africa. *Geophys. Res. Lett.*, **42**, 8208–8215, https://doi.org/10.1002/2015GL065819.

Cuesta, J., J. H. Marsham, D. J. Parker, and C. Flamant, 2009: Dynamical mechanisms controlling the vertical redistribution of dust and the thermodynamic structure of the West Saharan atmospheric boundary layer during summer. *Atmos. Sci. Lett.*, **10**, 34–42, https://doi.org/10.1002/asl.207.

Darmenova, K., I. N. Sokolik, Y. Shao, B. Marticorena, and G. Bergametti, 2009: Development of a physically based dust emission module within the Weather Research and Forecasting (WRF) Model: Assessment of dust emission parameterizations and input parameters for source regions in Central and East Asia. *J. Geophys. Res.*, **114**, D14201, https://doi.org/10.1029/2008JD011236.

DeMott, P. J., K. Sassen, M. R. Poellot, D. Baumgardner, D. C. Rogers, S. D. Brooks, A. J. Prenni, and S. M. Kreidenweis, 2003: African dust aerosols as atmospheric ice nuclei. *Geophys. Res. Lett.*, **30**, 1732, https://doi.org/10.1029/2003GL017410.

Drager, A. J., and S. C. van den Heever, 2017: Characterizing convective cold pools. *J. Adv. Model. Earth Syst.*, **9**, 1091–1115, https://doi.org/10.1002/2016MS000788.

——, L. D. Grant, and S. C. van den Heever, 2020: Cold pool responses to changes in soil moisture. *J. Adv. Model.*

Earth Syst., **12**, e2019MS001922, https://doi.org/10.1029/2019MS001922.

Droegemeier, K. K., and R. B. Wilhelmson, 1987: Numerical simulation of thunderstorm outflow dynamics. Part I: Outflow sensitivity experiments and turbulence dynamics. *J. Atmos. Sci.*, **44**, 1180–1210, https://doi.org/10.1175/1520-0469(1987)044<1180:NSOTOD>2.0.CO;2.

Emmel, C., P. Knippertz, and O. Schulz, 2010: Climatology of convective density currents in the southern foothills of the Atlas Mountains. *J. Geophys. Res.*, **115**, D11115, https://doi.org/10.1029/2009JD012863.

Fast, J. D., L. K. Berg, Z. Feng, F. Mei, R. Newsom, K. Sakaguchi, and H. Xiao, 2019: The impact of variable land-atmosphere coupling on convective cloud populations observed during the 2016 HI-SCALE field campaign. *J. Adv. Model. Earth Syst.*, **11**, 2629–2654, https://doi.org/10.1029/2019MS001727.

Fécan, F., B. Marticorena, and G. Bergametti, 1999: Parameterization of the increase of the aeolian erosion threshold wind friction velocity due to soil moisture for arid and semi-arid areas. *Ann. Geophys.*, **17**, 149–157, https://doi.org/10.1007/s00585-999-0149-7.

Field, P. R., O. Möhler, P. Connolly, M. Krämer, R. Cotton, A. J. Heymsfield, H. Saathoff, and M. Schnaiter, 2006: Some ice nucleation characteristics of Asian and Saharan desert dust. *Atmos. Chem. Phys.*, **6**, 2991–3006, https://doi.org/10.5194/acp-6-2991-2006.

Flamant, C., J.-P. Chaboureau, D. J. Parker, C. M. Taylor, J. P. Cammas, O. Bock, F. Timouk, and J. Pelon, 2007: Airborne observations of the impact of a convective system on the planetary boundary layer thermodynamics and aerosol distribution in the intertropical discontinuity region of the West African monsoon. *Quart. J. Roy. Meteor. Soc.*, **133**, 1175–1189, https://doi.org/10.1002/qj.97.

Foroutan, H., J. Young, S. Napelenok, L. Ran, K. W. Appel, R. C. Gilliam, and J. E. Pleim, 2017: Development and evaluation of a physics-based windblown dust emission scheme implemented in the CMAQ modeling system. *J. Adv. Model. Earth Syst.*, **9**, 585–608, https://doi.org/10.1002/2016MS000823.

Garcia-Carreras, L., and Coauthors, 2015: The turbulent structure and diurnal growth of the Saharan atmospheric boundary layer. *J. Atmos. Sci.*, **72**, 693–713, https://doi.org/10.1175/JAS-D-13-0384.1.

Garcia Sanchez, D., B. Lacarrière, M. Musy, and B. Bourges, 2014: Application of sensitivity analysis in building energy simulations: Combining first- and second-order elementary effects methods. *Energy Build.*, **68**, 741–750, https://doi.org/10.1016/j.enbuild.2012.08.048.

Gentine, P., A. Garelli, S.-B. Park, J. Nie, G. Torri, and Z. Kuang, 2016: Role of surface heat fluxes underneath cold pools. *Geophys. Res. Lett.*, **43**, 874–883, https://doi.org/10.1002/2015GL067262.

Ginoux, P., M. Chin, I. Tegen, J. M. Prospero, B. Holben, O. Dubovik, and S.-J. Lin, 2001: Sources and distributions of dust aerosols simulated with the GOCART model. *J. Geophys. Res.*, **106**, 20 255–20 273, https://doi.org/10.1029/2000JD000053.

——, J. M. Prospero, O. Torres, and M. Chin, 2004: Long-term simulation of global dust distribution with the GOCART model: Correlation with North Atlantic Oscillation. *Environ. Modell. Software*, **19**, 113–128, https://doi.org/10.1016/S1364-8152(03)00114-2.

——, ——, T. E. Gill, N. C. Hsu, and M. Zhao, 2012: Global-scale attribution of anthropogenic and natural dust sources and their emission rates based on MODIS Deep Blue aerosol products. *Rev. Geophys.*, **50**, RG3005, https://doi.org/10.1029/2012RG000388.

Goudie, A. S., 2014: Desert dust and human health disorders. *Environ. Int.*, **63**, 101–113, https://doi.org/10.1016/j.envint.2013.10.011.

Grant, L. D., and S. C. van den Heever, 2016: Cold pool dissipation. *J. Geophys. Res. Atmos.*, **121**, 1138–1155, https://doi.org/10.1002/2015JD023813.

——, and ——, 2018: Cold pool-land surface interactions in a dry continental environment. *J. Adv. Model. Earth Syst.*, **10**, 1513–1526, https://doi.org/10.1029/2018MS001323.

Gyamfi, C., J. M. Ndambuki, and R. W. Salim, 2016: Spatial variability modeling of soil erodibility index in relation to some soil properties at field scale. *Environ. Nat. Resour. Res.*, **6**, 16–27, https://doi.org/10.5539/enrr.v6n2p16.

Harrington, J. Y., 1997: The effects of radiative and microphysical processes on simulated warm and transition season Arctic stratus. Ph.D. dissertation, Colorado State University, 301 pp.

Haywood, J., and Coauthors, 2003: Radiative properties and direct radiative effect of Saharan dust measured by the C-130 aircraft during SHADE: 1. Solar spectrum. *J. Geophys. Res.*, **108**, 8577, https://doi.org/10.1029/2002JD002687.

Heinold, B., P. Knippertz, J. H. Marsham, S. Fiedler, N. S. Dixon, K. Schepanski, B. Laurent, and I. Tegen, 2013: The role of deep convection and nocturnal low-level jets for dust emission in summertime West Africa: Estimates from convection-permitting simulations. *J. Geophys. Res. Atmos.*, **118**, 4385–4400, https://doi.org/10.1002/jgrd.50402.

Hill, G. E., 1974: Factors controlling the size and spacing of cumulus clouds as revealed by numerical experiments. *J. Atmos. Sci.*, **31**, 646–673, https://doi.org/10.1175/1520-0469(1974)031<0646:FCTSAS>2.0.CO;2.

Hirt, M., G. C. Craig, S. A. K. Schäfer, J. Savre, and R. Heinze, 2020: Cold-pool-driven convective initiation: Using causal graph analysis to determine what convection-permitting models are missing. *Quart. J. Roy. Meteor. Soc.*, **146**, 2205–2227, https://doi.org/10.1002/qj.3788.

Huang, Q., J. H. Marsham, W. Tian, D. J. Parker, and L. Garcia-Carreras, 2018: Large-eddy simulation of dust-uplift by a haboob density current. *Atmos. Environ.*, **179**, 31–39, https://doi.org/10.1016/j.atmosenv.2018.01.048.

Jeevanjee, N., 2017: Vertical velocity in the gray zone. *J. Adv. Model. Earth Syst.*, **9**, 2304–2316, https://doi.org/10.1002/2017MS001059.

Jickells, T., and C. M. Moore, 2015: The importance of atmospheric deposition for ocean productivity. *Annu. Rev. Ecol. Evol. Syst.*, **46**, 481–501, https://doi.org/10.1146/annurev-ecolsys-112414-054118.

Knippertz, P., and M. C. Todd, 2012: Mineral dust aerosols over the Sahara: Meteorological controls on emission and transport and implications for modeling. *Rev. Geophys.*, **50**, RG1007, https://doi.org/10.1029/2011RG000362.

——, C. Deutscher, K. Kandler, T. Müller, O. Schulz, and L. Schütz, 2007: Dust mobilization due to density currents in the Atlas region: Observations from the Saharan Mineral Dust Experiment 2006 field campaign. *J. Geophys. Res.*, **112**, D21109, https://doi.org/10.1029/2007JD008774.

——, J. Trentmann, and A. Seifert, 2009: High-resolution simulations of convective cold pools over the northwestern Sahara. *J. Geophys. Res.*, **114**, D08110, https://doi.org/10.1029/2008JD011271.

Knopf, D. A., and T. Koop, 2006: Heterogeneous nucleation of ice on surrogates of mineral dust. *J. Geophys. Res.*, **111**, D12201, https://doi.org/10.1029/2005JD006894.

Kok, J. F., 2011: A scaling theory for the size distribution of emitted dust aerosols suggests climate models underestimate the size of the global dust cycle. *Proc. Natl. Acad. Sci. USA*, **108**, 1016–1021, https://doi.org/10.1073/pnas.1014798108.

——, E. J. R. Parteli, T. I. Michaels, and D. Bou Karam, 2012: The physics of wind-blown sand and dust. *Rep. Prog. Phys.*, **75**, 106901, https://doi.org/10.1088/0034-4885/75/10/106901.

Kurowski, M. J., K. Suselj, W. W. Grabowski, and J. Teixeira, 2018: Shallow-to-deep transition of continental moist convection: Cold pools, surface fluxes, and mesoscale organization. *J. Atmos. Sci.*, **75**, 4071–4090, https://doi.org/10.1175/JAS-D-18-0031.1.

Lawson, T., 1971: Haboob structure at Khartoum. *Weather*, **26**, 105–112, https://doi.org/10.1002/j.1477-8696.1971.tb07402.x.

Lebo, Z. J., and H. Morrison, 2015: Effects of horizontal and vertical grid spacing on mixing in simulated squall lines and implications for convective strength and structure. *Mon. Wea. Rev.*, **143**, 4355–4375, https://doi.org/10.1175/MWR-D-15-0154.1.

Lee, J. A., M. C. Baddock, M. J. Mbuh, and T. E. Gill, 2012: Geomorphic and land cover characteristics of aeolian dust sources in West Texas and eastern New Mexico, USA. *Aeolian Res.*, **3**, 459–466, https://doi.org/10.1016/j.aeolia.2011.08.001.

LeGrand, S. L., C. Polashenski, T. W. Letcher, G. A. Creighton, S. E. Peckham, and J. D. Cetola, 2019: The AFWA dust emission scheme for the GOCART aerosol model in WRF-Chem v3.8.1. *Geosci. Model Dev.*, **12**, 131–166, https://doi.org/10.5194/gmd-12-131-2019.

Lilly, D. K., 1962: On the numerical simulation of buoyant convection. *Tellus*, **14**, 148–172, https://doi.org/10.3402/tellusa.v14i2.9537.

Liu, C., and M. W. Moncrieff, 2000: Simulated density currents in idealized stratified environments. *Mon. Wea. Rev.*, **128**, 1420–1437, https://doi.org/10.1175/1520-0493(2000)128<1420:SDCIIS>2.0.CO;2.

MacKinnon, D. J., G. D. Clow, R. K. Tigges, R. L. Reynolds, and P. S. Chaves Jr., 2004: Comparison of aerodynamically and model-derived roughness lengths (z_0) over diverse surfaces, central Mojave Desert, California, USA. *Geomorphology*, **63**, 103–113, https://doi.org/10.1016/j.geomorph.2004.03.009.

Mahowald, N., and Coauthors, 2005: Atmospheric global dust cycle and iron inputs to the ocean. *Global Biogeochem. Cycles*, **19**, GB4025, https://doi.org/10.1029/2004GB002402.

——, and Coauthors, 2010: Observed 20th century desert dust variability: Impact on climate and biogeochemistry. *Atmos. Chem. Phys.*, **10**, 10 875–10 893, https://doi.org/10.5194/acp-10-10875-2010.

——, S. Albani, J. F. Kok, S. Engelstaeder, R. Scanza, D. S. Ward, and M. G. Flanner, 2014: The size distribution of desert dust aerosols and its impact on the Earth system. *Aeolian Res.*, **15**, 53–71, https://doi.org/10.1016/j.aeolia.2013.09.002.

Marsham, J. H., and Coauthors, 2013: Meteorology and dust in the central Sahara: Observations from Fennec supersite-1 during the June 2011 intensive observation period. *J. Geophys. Res. Atmos.*, **118**, 4069–4089, https://doi.org/10.1002/jgrd.50211.

Marticorena, B., and G. Bergametti, 1995: Modeling the atmospheric dust cycle: 1. Design of a soil-derived dust emission scheme. *J. Geophys. Res.*, **100**, 16 415–16 430, https://doi.org/10.1029/95JD00690.

——, and Coauthors, 2006: Surface and aerodynamic roughness in arid and semiarid areas and their relation to radar backscatter coefficient. *J. Geophys. Res.*, **111**, F03017, https://doi.org/10.1029/2006JF000462.

Martin, J. H., 1991: Iron still comes from above. *Nature*, **353**, 123, https://doi.org/10.1038/353123b0.

Membery, D. A., 1985: A gravity-wave haboob? *Weather*, **40**, 214–221, https://doi.org/10.1002/j.1477-8696.1985.tb06877.x.

Mesinger, F., and A. Arakawa, 1976: Numerical methods used in atmospheric models. WMO GARP Publ. 17, Vol. 1, 66 pp.

Middleton, N. J., 2017: Desert dust hazards: A global review. *Aeolian Res.*, **24**, 53–63, https://doi.org/10.1016/j.aeolia.2016.12.001.

——, and U. Kang, 2017: Sand and dust storms: Impact mitigation. *Sustainability*, **9**, 1053, https://doi.org/10.3390/su9061053.

Miller, S. D., A. P. Kuciauskas, M. Liu, Q. Ji, J. S. Reid, D. W. Breed, A. L. Walker, and A. A. Mandoos, 2008: Haboob dust storms of the southern Arabian Peninsula. *J. Geophys. Res.*, **113**, D01202, https://doi.org/10.1029/2007JD008550.

——, and Coauthors, 2019: A tale of two dust storms: Analysis of a complex dust event in the Middle East. *Atmos. Meas. Tech.*, **12**, 5101–5118, https://doi.org/10.5194/amt-12-5101-2019.

Mokhtari, M., L. Gomes, P. Tulet, and T. Rezoug, 2012: Importance of the surface size distribution of erodible material: An improvement on the Dust Entrainment And Deposition (DEAD) model. *Geosci. Model Dev.*, **5**, 581–598, https://doi.org/10.5194/gmd-5-581-2012.

Morris, M. D., 1991: Factorial sampling plans for preliminary computational experiments. *Technometrics*, **33**, 161–174, https://doi.org/10.1080/00401706.1991.10484804.

Munson, S. M., J. Belnap, and G. S. Okin, 2011: Responses of wind erosion to climate-induced vegetation changes on the Colorado Plateau. *Proc. Natl. Acad. Sci. USA*, **108**, 3854–3859, https://doi.org/10.1073/pnas.1014947108.

Neff, J. C., and Coauthors, 2008: Increasing eolian dust deposition in the western United States linked to human activity. *Nat. Geosci.*, **1**, 189–195, https://doi.org/10.1038/ngeo133.

Pantillon, F., P. Knippertz, J. H. Marsham, and C. E. Birch, 2015: A parameterization of convective dust storms for models with mass-flux convection schemes. *J. Atmos. Sci.*, **72**, 2545–2561, https://doi.org/10.1175/JAS-D-14-0341.1.

——, ——, ——, H. Panitz, and I. Bischoff-Gauss, 2016: Modeling haboob dust storms in large-scale weather and climate models. *J. Geophys. Res. Atmos.*, **121**, 2090–2109, https://doi.org/10.1002/2015JD024349.

Pianosi, F., F. Sarrazin, and T. Wagener, 2015: A MATLAB toolbox for global sensitivity analysis. *Environ. Modell. Software*, **70**, 80–85, https://doi.org/10.1016/j.envsoft.2015.04.009.

——, K. Beven, J. Freer, J. W. Hall, J. Rougier, D. B. Stephenson, and T. Wagener, 2016: Sensitivity analysis of environmental models: A systematic review with practical workflow. *Environ. Modell. Software*, **79**, 214–232, https://doi.org/10.1016/j.envsoft.2016.02.008.

Pielke, R. A., and Coauthors, 1992: A comprehensive meteorological modeling system—RAMS. *Meteor. Atmos. Phys.*, **49**, 69–91, https://doi.org/10.1007/BF01025401.

Pierre, C., G. Bergametti, B. Marticorena, E. Mougin, C. Bouet, and C. Schmechtig, 2012: Impact of vegetation and soil moisture seasonal dynamics on dust emissions over the Sahel. *J. Geophys. Res.*, **117**, D06114, https://doi.org/10.1029/2011JD016950.

Provod, M., J. H. Marsham, D. J. Parker, and C. E. Birch, 2016: A characterization of cold pools in the West African Sahel.

Mon. Wea. Rev., **144**, 1923–1934, https://doi.org/10.1175/MWR-D-15-0023.1.

Reheis, M. C., and F. E. Urban, 2011: Regional and climatic controls on seasonal dust deposition in the southwestern U.S. *Aeolian Res.*, **3**, 3–21, https://doi.org/10.1016/j.aeolia.2011.03.008.

Rempel, A. R., and A. W. Rempel, 2016: Intrinsic evaporative cooling by hygroscopic Earth materials. *Geosciences*, **6**, 38, https://doi.org/10.3390/geosciences6030038.

Roberts, A. J., and P. Knippertz, 2012: Haboobs: Convectively generated dust storms in West Africa. *Weather*, **67**, 311–316, https://doi.org/10.1002/wea.1968.

——, and ——, 2014: The formation of a large summertime Saharan dust plume: Convective and synoptic-scale analysis. *J. Geophys. Res. Atmos.*, **119**, 1766–1785, https://doi.org/10.1002/2013JD020667.

Rotunno, R., J. B. Klemp, and M. L. Weisman, 1988: A theory for strong, long-lived squall lines. *J. Atmos. Sci.*, **45**, 463–485, https://doi.org/10.1175/1520-0469(1988)045<0463:ATFSLL>2.0.CO;2.

Saleeby, S. M., and S. C. van den Heever, 2013: Developments in the CSU-RAMS aerosol model: Emissions, nucleation, regeneration, deposition, and radiation. *J. Appl. Meteor. Climatol.*, **52**, 2601–2622, https://doi.org/10.1175/JAMC-D-12-0312.1.

——, and Coauthors, 2019: The influence of simulated surface dust lofting and atmospheric loading on radiative forcing. *Atmos. Chem. Phys.*, **19**, 10 279–10 301, https://doi.org/10.5194/acp-19-10279-2019.

Saltelli, A., S. Tarantola, F. Campolongo, and M. Ratto, 2004: *Sensitivity Analysis in Practice: A Guide to Assessing Scientific Models*. 1st ed. John Wiley and Sons, 232 pp.

Sarrazin, F., F. Pianosi, and T. Wagener, 2016: Global sensitivity analysis of environmental models: Convergence and validation. *Environ. Modell. Software*, **79**, 135–152, https://doi.org/10.1016/j.envsoft.2016.02.005.

Sayre, R., and Coauthors, 2020: An assessment of the representation of ecosystems in global protected areas using new maps of world climate regions and world ecosystems. *Global Ecol. Conserv.*, **21**, e00860, https://doi.org/10.1016/j.gecco.2019.e00860.

Seigel, R. B., and S. C. van den Heever, 2012a: Simulated density currents beneath embedded stratified layers. *J. Atmos. Sci.*, **69**, 2192–2200, https://doi.org/10.1175/JAS-D-11-0255.1.

——, and ——, 2012b: Dust lofting and ingestion by supercell storms. *J. Atmos. Sci.*, **69**, 1453–1473, https://doi.org/10.1175/JAS-D-11-0222.1.

Seinfeld, J. H., and S. N. Pandis, 2006: *Atmospheric Chemistry and Physics: From Air Pollution to Climate Change*. John Wiley and Sons, 1203 pp.

Shao, Y., 2001: A model for mineral dust emission. *J. Geophys. Res.*, **106**, 20 239–20 254, https://doi.org/10.1029/2001JD900171.

——, 2004: Simplification of a dust emission scheme and comparison with data. *J. Geophys. Res.*, **109**, D10202, https://doi.org/10.1029/2003JD004372.

——, and H. Lu, 2000: A simple expression for wind erosion threshold friction velocity. *J. Geophys. Res.*, **105**, 22 437–22 443, https://doi.org/10.1029/2000JD900304.

——, and Y. Yang, 2005: A scheme for drag partition over rough surfaces. *Atmos. Environ.*, **39**, 7351–7361, https://doi.org/10.1016/j.atmosenv.2005.09.014.

——, M. R. Raupach, and J. F. Leys, 1996: A model for predicting aeolian sand drift and dust entrainment on scales from paddock to region. *Aust. J. Soil Res.*, **34**, 309–342, https://doi.org/10.1071/SR9960309.

——, E. Jung, and L. Leilie, 2002: Numerical prediction of northeast Asian dust storms using an integrated wind erosion modeling system. *J. Geophys. Res.*, **107**, 4814, https://doi.org/10.1029/2001JD001493.

——, M. Ishizuka, M. Mikami, and J. F. Leys, 2011: Parameterization of size-resolved dust emission and validation with measurements. *J. Geophys. Res.*, **116**, D08203, https://doi.org/10.1029/2010JD014527.

Slingo, A., and Coauthors, 2006: Observations of the impact of a major Saharan dust storm on the atmospheric radiation balance. *Geophys. Res. Lett.*, **33**, L24817, https://doi.org/10.1029/2006GL027869.

Smagorinsky, J., 1963: General circulation experiments with the primitive equations. I. The basic experiment. *Mon. Wea. Rev.*, **91**, 99–164, https://doi.org/10.1175/1520-0493(1963)091<0099:GCEWTP>2.3.CO;2.

Smith, M. A., 2007: Evaluation of mesoscale simulations of dust sources, sinks, and transport over the Middle East. M.S. thesis, Dept. of Atmospheric Science, Colorado State University, 126 pp.

Soil Survey Staff, 1999: Soil taxonomy: A basic system of soil classification for making and interpreting soil surveys. USDA NRCS Agriculture Handbook 436, 870 pp.

Sokolik, I. N., and O. B. Toon, 1996: Direct radiative forcing by anthropogenic airborne mineral aerosols. *Nature*, **381**, 681–683, https://doi.org/10.1038/381681a0.

Sprigg, W. A., 2016: Dust storms, human health and a global early warning system. *Extreme Weather, Health, and Communities. Extreme Weather and Society*, S. Steinberg and W. Sprigg, Eds., Springer, 59–87, https://doi.org/10.1007/978-3-319-30626-1_4.

Stokowski, D., 2005: The addition of the direct radiative effect of atmospheric aerosols into the Regional Atmospheric Modeling System (RAMS). M.S. thesis, Dept. of Atmospheric Science, Colorado State University, 89 pp.

Stout, J. E., 2001: Dust and environment in the Southern High Plains of North America. *J. Arid Environ.*, **47**, 425–441, https://doi.org/10.1006/jare.2000.0732.

Straka, J. M., R. B. Wilhelmson, L. J. Wicker, J. R. Anderson, and K. K. Droegemeier, 1993: Numerical solutions of a nonlinear density current: A benchmark solution and comparisons. *Int. J. Numer. Methods Fluids*, **17**, 1–22, https://doi.org/10.1002/fld.1650170103.

Tanaka, T. Y., and M. Chiba, 2006: A numerical study of the contributions of dust source regions to the global dust budget. *Global Planet. Change*, **52**, 88–104, https://doi.org/10.1016/j.gloplacha.2006.02.002.

Trzeciak, T. M., L. Garcia-Carreras, and J. H. Marsham, 2017: Cross-Saharan transport of water vapor via recycled cold pool outflows from moist convection. *Geophys. Res. Lett.*, **44**, 1554–1563, https://doi.org/10.1002/2016GL072108.

Ukhov, A., R. Ahmadov, G. Grell, and G. Stenchikov, 2021: Improving dust simulations in WRF-Chem v4.1.3 coupled with the GOCART aerosol module. *Geosci. Model Dev.*, **14**, 473–493, https://doi.org/10.5194/gmd-14-473-2021.

Vaezi, A. R., H. Hasanzadeh, and A. Cerdà, 2016: Developing an erodibility triangle for soil textures in semi-arid regions, NW Iran. *Catena*, **142**, 221–232, https://doi.org/10.1016/j.catena.2016.03.015.

van den Heever, S. C., and Coauthors, 2021: The Colorado State University Convective Cloud Outflows and Updrafts Experiment (C^3LOUD-Ex). *Bull. Amer. Meteor. Soc.*, **102**, E1283–E1305, https://doi.org/10.1175/BAMS-D-19-0013.1.

Walker, A. L., M. Liu, S. D. Miller, K. A. Richardson, and D. L. Westphal, 2009: Development of a dust source database for mesoscale forecasting in southwest Asia. *J. Geophys. Res.*, **114**, D18207, https://doi.org/10.1029/2008JD011541.

Walko, R. L., and Coauthors, 2000: Coupled atmosphere–biophysics–hydrology models for environmental modeling. *J. Appl. Meteor.*, **39**, 931–944, https://doi.org/10.1175/1520-0450(2000)039<0931:CABHMF>2.0.CO;2.

Webb, N. P., A. Chappell, S. L. LeGrand, N. P. Ziegler, and B. L. Edwards, 2020: A note on the use of drag partition in aeolian transport models. *Aeolian Res.*, **42**, 100560, https://doi.org/10.1016/j.aeolia.2019.100560.

Xi, X., and I. N. Sokolik, 2015: Seasonal dynamics of threshold friction velocity and dust emission in Central Asia. *J. Geophys. Res. Atmos.*, **120**, 1536–1564, https://doi.org/10.1002/2014JD022471.